**Climate Dynamics manuscript No.**
(will be inserted by the editor)

# The double ITCZ bias in CMIP5 models: interaction between SST, large-scale circulation and precipitation

**Boutheina Oueslati and Gilles Bellon**

Received: date / Accepted: date

**Abstract** The double Intertropical Convergence Zone (ITCZ) syndrome still affects all the models that participate to CMIP5 (Coupled Model Intercomparaison Project, phase 5). As an ensemble, general circulation models have improved little between CMIP3 and CMIP5 as far as the double ITCZ is concerned. The aim of this study is to investigate the respective roles of coupled ocean-atmosphere and large-scale atmospheric mechanisms in the double ITCZ problem. The SST contribution is examined using the THR-MLT index (Bellucci et al, 2010), which combines biases on the representation of local SSTs (MLT) and the SST threshold leading to the onset of ascent (THR) in the double ITCZ region. We introduce a metric of the model misrepresentation of the relationship between large-scale circulation and convection, that we call "Combined Precipitation Circulation Error (CPCE)". It measures the combined biases on the simulated frequency of occurrence of vertical-motion regimes and on the rainfall magnitude simulated in each dynamical regime in the tropics. A linear regression analysis shows that most of the double ITCZ spread among CMIP5 coupled ocean-atmosphere models can be attributed to coupled processes, and that the interaction between precipitation and large-scale dynamics explains a significant fraction of the bias in these models, as well as in the atmosphere-only models.

**Keywords** Double ITCZ · Atmospheric dynamics · Coupled ocean-atmosphere feedbacks

---

B. Oueslati

Centre National de Recherches Météorologiques, CNRS/Météo-France, 42, avenue Gaspard Coriolis, 31057 Toulouse Cedex 01, France.

E-mail: boutheina.oueslati@meteo.fr.

## 1 Introduction

Most current general circulation models (GCMs) still suffer from the double intertropical convergence zone (ITCZ) syndrome (Mechoso et al, 1995; Dai, 2006). They fail to simulate the position of the ITCZ north of the equator year-round. Instead, they produce a second maximum of precipitation south of the equator in the eastern Pacific during at least half of the year, whereas it is only observed during boreal spring (Hubert et al, 1969; Zhang, 2001). The double ITCZ bias also affects the central Pacific and it can be connected to the simulation of a too-zonally elongated South Pacific Convergence Zone (SPCZ).

Both atmospheric and coupled ocean-atmosphere processes play an important role in controlling the ITCZ location. The Sea surface temperature (SST) affects convection by supplying heat and moisture to the atmospheric column through the turbulent surface fluxes, and by creating low-level convergence through its gradients (Lindzen and Nigam, 1987; Back and Bretherthon, 2008; Oueslati and Bellon, 2013a). The spatial distribution of SST is however poorly simulated in coupled ocean-atmosphere GCMs (OAGCMs), with a positive SST bias over the southeastern Pacific and an excessive equatorial cold tongue extending too far west in the Pacific. These biases are attributed to coupled ocean-atmosphere feedbacks such as the SST-wind-induced surface fluxes feedback, the SST-stratus feedback and the SST gradient-trade wind feedback associated with vertical upwelling (Lin, 2007).

Together with the SST's control, atmospheric mechanisms are crucial in determining the ITCZ location. Because the diabatic heating associated with convection changes the pressure gradients, deep convection forces circulations. Vice-versa, low-level convergence can provide the humidity necessary for convection, so that the feedbacks between dynamics and moist thermodynamics are instrumental in controlling the precipitation pattern. Based on the conditional instability of the second kind (CISK) theory (Charney, 1971) and the associated wave-CISK mechanisms (Holton et al, 1971; Lindzen, 1974; Hess et al, 1993), early studies emphasized the role of convection-large-scale convergence feedback to explain the ITCZ location. Atmospheric dynamics promote convection through large-scale upward motions, associated with moisture convergence, but it can also suppress convection through large-scale subsidence (Lau et al, 1997; Xie et al, 2010). Subsequent studies highlighted the importance of the interaction between convection and its large-scale environment on the basis of the quasi-equilibrium theory (Arakawa and Schubert, 1974; Emanuel, 1994). According to this theory, both dynamical and thermodynamical processes control the convective activity and, thus, the ITCZ location. In particular, Numaguti (1993) showed that the ITCZ structure is sensitive to the surface-flux parameterization and Liu et al (2010) associated the double ITCZ obtained in aquaplanet settings with the wind-evaporation feedback. The quasi-equilibrium theory *per se* does not provide a systematic mechanism of interaction between precipitation and dynamics.

The ITCZ pattern is very sensitive to the deep-convection scheme and parameters because they determine the response of the convection to given large-scale environment and forcings, and also because they control the dynamic response to convection through the vertical profile of convective heating. Rain reevaporation (Bacmeister et al, 2006), cold top and downdrafts (Oueslati and Bellon, 2013a) and lateral entrainment (Chikira, 2010; Hirota et al, 2011; Oueslati and Bellon, 2013b) can all have an impact on the precipitation pattern. In particular, sensitivity studies to convective entrainment using the CNRM-CM5 hierarchy of models show that, in that model, the double ITCZ bias is associated with an error in the probability density function (PDF) of mid-tropospheric vertical wind resulting from feedbacks between dynamics and convection (Oueslati and Bellon, 2013b).

The purpose of this study is to quantify the respective roles of SST and large-scale dynamics in the double ITCZ problem in OAGCMs and, when available, corresponding atmosphere-only GCMs (AGCMs) participating to CMIP5 (Coupled Model Intercomparaison Project, phase 5). The SST contribution is analyzed following Bellucci et al (2010). The large-scale atmospheric contribution is examined using the regime sorting methodology developed by Bony et al (2004). These two contributions are quantified based on a linear regression analysis. Using this statistical method, we attempt to show that the double ITCZ bias is associated not only with biases of the local SSTs (Bellucci et al, 2010) but also with the systematic errors affecting the large-scale atmospheric circulation.

The paper is structured as follows. In section 2, we introduce the models used for this study. In section 3, we investigate the CMIP5 OAGCMs systematic errors in tropical precipitation. Section 4 quantifies the role of SST and associated coupled ocean-atmosphere feedbacks in the double ITCZ syndrom. Section 5 investigates the contribution of precipitation/dynamics interaction to this systematic bias. The respective roles of the coupled ocean-atmosphere processes and atmospheric precipitation/dynamics processes are quantified in section 6. Summary and conclusions are given in section 7.

## 2 CMIP5 models

We use the monthly outputs of 21 years (1979-1999) of the reference historical simulations performed for CMIP5 (referred to as CMIP). They are currently available for 17 OAGCMs. In addition, we use the corresponding atmosphere-only simulations (commonly referred to as Atmospheric Model Intercomparaison Project (AMIP) simulations), with prescribed SST and interactive continental surfaces. These AMIP simulations are available for 13 AGCMs out of the 17 OAGCMs. Table 1 summarizes the characteristics of the models used in this study with their names and acronyms, their horizontal and vertical resolutions and a brief description of their deep convection schemes. For simplicity, we refer to each model by the name of its institution in figure legends.

Model results are compared with observational datasets and reanalyses (referred to as OBS in figure legends). In particular, the Global Precipitation Climatology Project (GPCP) version 2 precipitation dataset (Adler et al, 2003) is used for precipitation. The 40-yr ECMWF Re-analysis (ERA40) is used for the mid-tropospheric vertical speed $\omega_{500}$ fields. The global Hadley Centre Global Sea Ice and Sea Surface Temperature (HadISST) analyses (Rayner et al, 2003) are used for sea surface temperatures (SST).

**Table 1** List of models analyzed in this study

| Modeling groups | IPCC ID | Atmospheric resolution | Deep convection scheme | Closure/trigger |
|---|---|---|---|---|
| National Center for Atmospheric Research (NCAR) | CCSM4 | $\simeq$ 0.9°x 1.25°-L26 | Revised Zhang and McFarlane (1995): Neale et al. (2008) , Richter and Rash (2008) | ”Dilute” CAPE |
| Canadian Centre for Climate Modeling and Analysis (CCCMA) | CanESM2 CanAM4 (AGCM) | T63-L35 | Zhang and McFarlane (1995) | CAPE |
| LASG-IAP/LASG, Institute of Atmospheric Physics, Chinese Academy of Sciences (IAP) | FGOALS-g2 | $\simeq$ 2.5°x 4°-L26 | Zhang and McFarlane (1995) | CAPE |
| NASA Goddard Institute for Space Studies (GISS) | GISS-E2-R | $\simeq$ 2°x 2.5°-L40 | Del Genio and Yao (1993) | A Cloud base neutral buoyancy/Parcel buoyancy |
| Beijing Climate Center, China Meteorological Administration (BCC) | BCC-CSM1-1 | T42-L26 | Revised Zhang and McFarlane (1995): Zhang and Mu (2005) | CAPE/Relative humidity threshold |
| Centre National de Recherches Meteorologiques (CNRM) | CNRM-CM5 | T127-L31 | Bougeault (1985) | Kuo/Conditional instability |
| Atmosphere and Ocean Research Institute (The University of Tokyo), National Institute for Environmental Studies, and Japan Agency for Marine-Earth Science and Technology (MIROC) | MIROC5 | T85-L40 | Chikira and Sugiyama (2010) | Prognostic convective kinetic energy |
| Met Office Hadley Centre (MOHC) | HadGEM2-ES HadGEM2-A (AGCM) | $\simeq$ 1.25°x 1.875°-L38 | Revised Gregory and Rowntree (1990) + Buoyancy-dependent Detrainment (Derbyshire et al. (submitted)) | Stability-dependent mass-flux/Parcel buoyancy |
| Commonwealth Scientific and Industrial Research Organisation in collaboration with the Queensland Climate Change Centre of Excellence (CSIRO) | CSIRO-Mk3-6-0 | T63-L18 | Gregory and Rowntree (1990) | Stability-dependent mass-flux/Parcel buoyancy |
| Meteorological Research Institute (MRI) | MRI-CGCM3 | TL159-L48 | Pan and Randall (1998) | Prognostic convective kinetic energy |
| Geophysical Fluid Dynamics Laboratory (GFDL) | GFDL-ESM2M GFDL-HIRAM-C360 (AGCM) | $\simeq$ 2.5°x 2°-L24 | Moorthi and Suarez (1992) | CAPE/Relative humidity Threshold |
| Max Planck Institute for Meteorology (MPI) | MPI-ESM-LR | $\simeq$ 1.9°x 1.9°-L47 | Nordeng (1994) | CAPE |
| Institute for Numerical Mathematics (INM) | INMCM4 | $\simeq$ 1.5°x 2°-L21 | Betts (1986) | CAPE |
| Institut Pierre-Simon Laplace (IPSL) | IPSL-CM5A-LR | $\simeq$ 1.9°x 3.75°-L39 | Emanuel (1991) | CAPE |
| | IPSL-CM5A-MR | $\simeq$ 1.25°x 2.5°-L39 | Emanuel (1991) | CAPE |
| | IPSL-CM5B-LR | $\simeq$ 1.9°x 3.75°-L39 | Grandpeix and Lafore (2010) Grandpeix et al (2010) | Available Lifting Power/ Available Lifting Energy |
| Norwegian Climate Centre (NCC) | NorESM1-M | $\simeq$ 1.8°x 2.5°-L26 | Zhang and McFarlane (1995) | CAPE |

# 3 Precipitation patterns in CMIP5 OAGCMs

## 3.1 Annual mean precipitation

Figure 1 shows the annual mean precipitation over the period 1979-1999 from GPCP v2 precipitation dataset Adler et al (2003) and 17 CMIP5 OAGCMs. All the models still produce the double ITCZ bias to some extent, with excessive precipitation south of the equator in the Pacific Ocean: the SPCZ is too-zonally elongated and a spurious ITCZ is simulated in the Eastern Pacific. In some models (e.g., GISS-E2-R and MRI-CGCM3), a double ITCZ pattern is also evident over the tropical Atlantic Ocean. Other model deficiencies still persist, including the excessive precipitation over the Maritime Continent, Indien Ocean, and within the Pacifc ITCZ, and the insufficient precipitation over the equator in the Pacific.

To quantify the double ITCZ bias over the tropical Pacific in GCMs, Bellucci et al. (2010) proposed a Southern ITCZ (SI) index, computed as the annual mean precipitation over the Double ITCZ region (20°S-0°, 100°- 150°W, referred to as the DI region). Figure 2 compares the SI index calculated for CMIP3 and CMIP5 models. It appears clearly that the double ITCZ bias is still present in all models. Only four modeling groups out of the 13 common ones between CMIP3 and CMIP5 improved their simulation of the annual mean precipitation in the southeastern Pacific. For the IPSL-CM5A, MPI-ESM-LR and CNRM-CM5, the improvement results in large part from an increase in resolution: the vertical resolution has been increased in IPSL-CM5A-LR and MPI-ESM-LR compared to the models in the CMIP3 generation, the horizontal resolution has been increased in CNRM-CM5 and both the horizontal and vertical resolutions have been increased in IPSL-CM5A-MR, but the convection parameterization in these models has not been significantly altered. IPSL-CM5B-LR and NCAR-CCSM4 also show an improvement in the SI index, and it can be explained by improvements of the existing parameterization of deep convection (Grandpeix and Lafore (2010) and Grandpeix et al (2010) for IPSL-CM5B-LR ; Neale et al (2008) for NCAR-CCSM4). In particular, in NCAR-CCSM4, two changes were made within the previous Zhang and McFarlane (1995) convection scheme. One is the inclusion of the effects of deep convection in the momentum equation (Richter and Rasch, 2008). The second is a modification of the calculation of convective available potential energy (CAPE), that has been reformulated to include more realistic dilution effects through an explicit representation of entrainment (Neale et al, 2008). Taking into account entrainment in cumulus parameterization strengthens the sensitivity of convection to the free-tropospheric humidity, resulting in a more constrained but vigourous precipitation (Neale et al, 2008; Oueslati and Bellon, 2013b). Compared to its CMIP3 version, MRI-CGCM3 no longer uses monthly climatological flux corrections, and this could explain the increase in SI index shown in figure 2.

Figure 3 shows the SI index computed from both CMIP5 OAGCMs and AGCMs. The double ITCZ bias is present in AMIP simulations. However, for the majority of models, its amplitude is smaller than in CMIP simulations. This is particularly the case of BCC-CSM1-1, GFDL-ESM2M and MRI-CGCM3. It appears, therefore, that coupled ocean-atmosphere feedbacks are still responsible for most of the double ITCZ bias in the East Pacific, maybe even more so than in the previous generation of models (Lin, 2007). This confirms that alleviating the double ITCZ bias in AGCMs is insufficient to solve the double ITCZ problem in OAGCMs as was suggested by the spread in the sensitivity of AGCMs and OAGCMs to convective entrainment (Oueslati and Bellon, 2013b).

## 3.2 Mean seasonal cycle

Figures 4 and 5 show the seasonal cycle of monthly precipitation averaged over two longitude sectors of the Pacific ocean from GPCP and for CMIP5 models. The seasonal cycle of the precipitation in the Eastern Pacific (80W-120W) has improved in some OAGCMs, as shown in Figure 4, compared to Dai (2006) and De Szoeke and Xie (2008) . De Szoeke and Xie (2008) divided the CMIP3 model into three main categories based on their seasonal cycle of precipitation. The first collects models displaying a persistent double ITCZ error in which rain persists too long in the Southern Hemisphere. The second collects models with an ITCZ and an SST maxima that cross the equator following the seasonal march of the insolation maximum. The third group collects models that are in qualitative agreement with the observed seasonal cycle, with the dominance of the northern ITCZ from May to December and the double ITCZ structure in March and April (see fig. 4 GPCP). This classification is still relevant for CMIP5 models, with improvements in some models. In particular, CNRM-CM5 and INMCM4 no longer simulate a double ITCZ all year-round (De Szoeke and Xie, 2008), but simulate a single ITCZ that moves across the equator following the solar forcing, similarly to the majority of CMIP5 models (IPSL-CM5, NCC-NorESM1-M, MPI-ESM-LR, CCCma-CanESM2,...). Two models (GISS-E2-R and IAP-FGOALS-g2) still exhibit a persistent double ITCZ error, with precipitation persisting year-round in the Southern Hemisphere. Three models (MIROC5, CSIRO-Mk3-6-0 and MOHC-HadGEM2-ES) reproduce qualitatively the observed seasonal cycle of precipitation. In MOHC-

HadGEM2-ES, however, the southern ITCZ is much more intense than in the observations ($\simeq 9$ mm day$^{-1}$ ), explaining the increase of the SI index from CMIP3 to CMIP5 (see fig. 2).

Over the Central Pacific (130W-170W), most of the models produce a persistent double ITCZ error with a southern rainbelt present throughout the year (see fig. 5). Only few models simulate qualitatively the seasonal cycle of the ITCZ, with no southern rainbelt in boreal summer (MIROC5, IPSL-CM5). However, it still persists too long compared to observations. In this region, the bias of simulated precipitation is in fact connected to the simulation of a too-zonally elongated SPCZ.

## 4 Coupled ocean-atmosphere contribution to the double ITCZ bias

In the tropics, organized convective activity is often colocated with warm SSTs. Warm SSTs cause large turbulent surface fluxes that increase low-level moist static energy and are favorable for convection. The SST also has a non local dynamical effect through its gradient that creates low-level convergence (Lindzen and Nigam, 1987; Back and Bretherthon, 2008; Oueslati and Bellon, 2013a). The modulation of the SST through coupled ocean-atmosphere feedbacks is therefore crucial to the precipitation pattern.

In this section, we focus on the role of the local SST control on precipitation, and particularly on the double ITCZ bias in southeastern Pacific in CMIP5 models, using the metrics proposed by Bellucci et al. (2010).

### 4.1 Description of the Bellucci index THR-MLT

The Bellucci et al. (2010) methodology is based on a regime-sorting analysis applied to SST in the DI region. The PDF of SST (bins of 0.5°C) is computed over the DI region (see fig. 6a). The SST corresponding to the maximum of the PDF is identified as the most likely temperature (MLT) of the ocean surface in the DI region (Bellucci et al, 2010). The average $\omega_{500}$ is computed for each 0.5°C SST bin over the DI region (see fig. 6b). An SST threshold (THR) corresponding to the SST at which $\omega_{500}$ (SST) changes sign is identified as the SST threshold leading to the onset of deep convection.

The difference THR-MLT between this SST threshold (THR) and the most likely SST over the DI region (MLT) is used to quantify the combined error of SSTs and local convection-SST coupling. This index determines whether the simulated regional oceanic conditions are favorable for the onset of deep convection given the model regional relationship between SST and convection. Positive (negative) values of THR-MLT correspond to models whose most frequent thermal conditions in the southeastern tropical Pacific are colder (warmer) than the deep convection threshold, producing therefore a less (more) pronounced double ITCZ (Bellucci et al, 2010).

4.2 The THR-MLT index in CMIP5 models: comparaison with CMIP3 models

Figure 6 shows SST PDFs (fig. 6a) and regime-sorted $\omega_{500}$ (fig. 6b) for the CMIP5 OAGCMs. Similarly to CMIP3 models, CMIP5 models exhibit lower THRs than the observed value (28°C). However, the THR spread between CMIP5 models is smaller, within 27°-28.5°C range compared to 26°-28.5°C range for CMIP3 models (see fig. 6b). The reduction of the spread is due to the improvement of three models: INMCM4, CNRM-CM5 and MIROC5, in which the THR has improved (27.5°C instead of 26.5°C in CMIP3 version). In particular, the more stringent threshold in MIROC5 might be explained by a modification in the parameterization of convective entrainment that tends to supress deep convection over dry, subsiding regions: Chikira and Sugiyama (2009) used an entrainment rate that depends on the buoyancy of the convective parcel, whereas the entrainment rate was originally uniform on the vertical.

The model SST shows a variety of distributions (see fig. 6a). In particular, IAP-FGOALS-g2 produces an SST distribution in better agreement with the observations than in its CMIP3 version. This is likely to result from improvements in the LASG/IAP Climate system Ocean Model (LICOM2), in the representation of some physical processes such as the vertical turbulent mixing, the solar radiation penetration and the mesoscale eddy parameterization as well as in the advection scheme (Liu et al, 2012).

The strong relationship between the THR-MLT index and the double ITCZ error, established in CMIP3 models (Bellucci et al, 2010), is also verified in CMIP5 models (see fig. 7), with positive THR-MLT corresponding to low double ITCZ error (e.g., MIROC5, NCC-NorESM1-M, IPSL-CM5A-MR) and negative THR-MLT corresponding to strong double ITCZ error (e.g., INMCM4, GISS-E2-R, MRI-CGCM3). The two indexes' correlation is -0.89, similar to the CMIP3 value of -0.84.

This linear relationship can be written as a simple regression between the measured variable (SI) and the explanatory variable (THR-MLT) as follows:

$$SI = \alpha_0 + \alpha_1\ (THR - MLT) + \epsilon, \tag{1}$$

where $\alpha_0 = SI_{OBS} - \alpha_1(THR - MLT)_{OBS} + \epsilon_0$ is the intercept, $\alpha_1 = -0.78$ mm day$^{-1}$ $°C^{-1}$ is the regression coefficient and $\epsilon$ is the residual. $\alpha_1$ is statistically significant with a p value smaller than $10^{-4}$ using Student's statistical test. The observed value is $SI_{OBS} - \alpha_1(THR - MLT)_{OBS} = 2.1$ mm day$^{-1}$ and $\epsilon_0 = 1.3$ mm day$^{-1}$ is the residual systematic error that is not accounted for by the error on THR-MLT. The regression results are summarized in Table 2.

To measure the goodness of fit of the statistical model defined by Equation (1) (i. e. how well the regression line fits the set of data), we look at the adjusted $R^2$ ($\overline{R^2}$)[1], that is estimated at 0.7 for CMIP5 AOGCMs. The strong relationship between the SI and the THR-MLT points out the importance of the thermodynamic forcing on precipitation in the DI region. This forcing is largely determined by local thermodynamic instability associated with warm SST and characterizes the local impact of SST on precipitation and the associated coupled ocean-atmosphere feedbacks. Figure 8 shows that the intermodel spread of THR-MLT is mostly due to that of MLT, and that the inter-model spread of THR has reduced between CMIP3 and CMIP5 models (see also fig. 6b) ; this suggests some convergence of AGCMs. However, OAGCMs still present a wide spectrum of SST distributions due to the various configurations of ocean models and the variety of coupled feedbacks. These results explain the enhanced inter-model spread in SI index in the coupled ocean-atmosphere simulations compared to the AMIP simulations (see fig. 3).

The relevance of THR-MLT highlights the local SST control on precipitation in CMIP5 models. However, it does not explain entirely the double ITCZ bias: the residual systematic error $\epsilon_0$ is significant. Also, since this index is mostly controlled by MLT, which is imposed in AMIP simulations, we can wonder whether this index can explain the spread in SI index in AMIP simulations. This will be investigated in section 4.3. Finally, some models with the same THR-MLT index, have different SI indexes (see fig. 7, e.g., IPSL-CM5B-LR and GFDL-ESM2M) ; it would be interesting to identify the mechanisms responsible for this spread.

[1] The coefficient of determination $R^2$ is the proportion of variability in a data set that is accounted for by the statistical model. It is defined as: $R^2 = \frac{\sum_i(\hat{SI}_i - \bar{SI}_i)^2}{\sum_i(SI_i - \bar{SI}_i)^2} = 1 - \frac{\sum_i(SI_i - \hat{SI}_i)^2}{\sum_i(SI_i - \bar{SI}_i)^2}$, where $SI$ is the observed value, $\hat{SI}$ is the predicted value by the regression model and $\bar{SI} = \frac{1}{n}\sum_i SI_i$. $\overline{R^2}$ is the proportion of variability in a data set that is accounted for by the statistical model, that accounts for the number of explanatory variables in the model. It is defined as: $\overline{R^2} = 1 - \frac{n-1}{n-p}\frac{\sum_i(SI_i - \hat{SI}_i)^2}{\sum_i(SI_i - \bar{SI}_i)^2}$.

### 4.3 The THR-MLT index in CMIP5 AGCMs

In this section, we apply the same regime analysis on the available CMIP5 AGCMs to investigate whether the relationship between the SI and THR-MLT indexes is verified in these models.

AMIP simulations are performed using observed SSTs as a lower boundary condition for the atmospheric model. All the models have, therefore, the same most likely thermal state MLT (see fig. 9a) ; a small difference in MLT can arise from the differing horizontal grids. The SST threshold THR for deep convection is still model-dependent. Vertical motions respond differently to imposed SST, resulting in a wide range of THR (see fig. 9b). THR-MLT is directly controlled by THR, in contrast with CMIP simulations in which it is strongly determined by model biases on SST (see fig. 8). The imposed oceanic conditions result in warmer THRs than in CMIP simulations and even than the observed THR for the majority of models (see fig. 9b). This suggests that ocean-atmosphere coupling has a positive feedback on convection, resulting in an easier onset of convection and a less constrained SST threshold in CMIP simulations (see fig. 6b).

Figure 10 shows the relationship between the SI index and THR-MLT in AMIP simulations. Again, the linear relationship between these two indexes is evident, but it is not as strong as in OAGCMs (SI and THR-MLT are correlated at the -0.76 level and $\overline{R^2}$ is 0.5). The linear regression between SI and THR-MLT, described by Equation (1) is performed for AGCMs. $\alpha_1$ is statistically significant (the p value of the corresponding statistical test is about $10^{-3}$) and is estimated at $-0.82$ mm day$^{-1}$ $^\circ C^{-1}$, similar to the estimation obtained for CMIP simulations. $\epsilon_0 = 0.86$ mm day$^{-1}$ is the residual systematic error that is not accounted for by the error on THR-MLT. The regression results are summarized in Table 2.

This regression shows that, even in the absence of coupled feedbacks, the THR-MLT index still contains some information on the SI index. This information results from the atmospheric mechanisms controlling THR among which feedbacks between precipitation and vertical motion play a prominent role. In the next section, we attempt to introduce a more complete measure of the error on the relationship between dynamics and precipitation and relate it to the SI index.

## 5 Large-scale atmospheric contribution to the double ITCZ

### 5.1 Large-scale dynamics control on precipitation

Large-scale circulation and precipitation interact strongly in the tropical atmosphere. On one hand, large-scale ascent is associated with moisture convergence and upward transport, both favorable for convection. On the other hand, large-scale subsidence, and sometimes horizontal advection, can suppress convection through the drying effect on the atmospheric boundary layer, that reduces its moist static energy (Lau et al, 1997; Xie et al, 2010), and on the free troposphere, that can damp the convective plumes through entrainment (Chikira, 2010; Hirota et al, 2011; Oueslati and Bellon, 2013b). Deep convection, in turn, modifies the temperature gradients through latent heat release in cumulus clouds (e.g., Gill, 1980) and convective cooling (Oueslati and Bellon, 2013a) ; the resulting pressure gradients force the large-scale circulation. The interaction between dynamics and precipitation is, therefore, at the heart of the atmospheric mechanisms that control the tropical precipitation patterns.

Many observational studies have documented the relationship between precipitation and large-scale dynamics. Analyzing the relationship between OLR (outgoing longwave radiation as a measure of convection) and SST, Lau et al. (1997) showed that the sensitivity of convection to local SST is strongly enhanced under strong large-scale upward motion within the 26-28$^\circ$C SST range. Above 28$^\circ$C, the intensity of convection is no longer dependent on the local SSTs, but it is more strongly controlled by the large-scale convergence (Graham and Barnet, 1987; Gutzler and Wood, 1990). In particular, a reduction in convection is observed in high SST "hot spot" situations which is likely to be explained by large-scale subsidence forced by nearby or remotely generated deep convection (Lau et al, 1997).

The sensitivity of convection to large-scale circulation is not well represented in GCMs. In fact, in the CMIP3 models the precipitation patterns follow the SST patterns too closely compared to observations, especially over the southeastern tropical Pacific (Lin, 2007). Hirota et al. (2011) argued that precipitation in models that overestimate precipitation in subsidence regions (e.g., the DI region) correlates strongly with SST and weakly with the large-scale circulation as diagnosed by $\omega_{500}$. The physical processes suppressing convection, that convey the influence of subsidence are still poorly represented in OAGCMs. In particular, the more realistic distribution of precipitation observed in both MIROC5 and NCAR-CCSM4 is attributed to a stronger circulation-precipitation interaction, resulting from modifications of the convection schemes, that take into account the large-scale processes in the calculation of entrainment (in the case of MIROC5, Hirota et al, 2011) and CAPE-based closure (in the case of NCAR-CCSM4, Song and Zhang, 2009). Using sensitivity studies, Oueslati and Bellon (2013b) showed that the double ITCZ is associated with errors in the PDF of $\omega_{500}$ and the errors on the contribution of each $\omega_{500}$ regime to the total precipitation. On the basis of this and the aforementioned studies, we introduce a measure of the errors on this contribution as a measure of the error on the precipitation-circulation relationship.

### 5.2 Combined Precipitation Circulation Error (CPCE) and the double ITCZ bias

To study the precipitation-large-scale circulation coupling and its role in the double ITCZ bias, we use the sorting methodology of Bony et al. (2004) in which the monthly-mean mid-tropospheric (500hPa) vertical pressure velocity $\omega_{500}$ is used as a proxy for large-scale ascent ($\omega_{500} < 0$) or subsidence ($\omega_{500} > 0$). The columns of the tropical atmosphere over oceans (30°S-30°N) are sorted into 10hPa bins of $\omega_{500}$. The resulting PDFs of $\omega_{500}$ are shown in figure 11a for ERA40 and for CMIP5 AGCMs. We also compute the average precipitation for each $\omega_{500}$ regime in the observations and in AGCMs (see fig. 11b). The contribution of each vertical regime to the total tropical precipitation is then quantified by weighting the regime-sorted precipitation by the PDF of $\omega_{500}$. The resulting distributions show the contribution of each dynamical regime to the mean tropical precipitation (see fig. 11c).

The CMIP5 AGCMs simulate a PDF of $\omega_{500}$ similar to the observed distribution in the tropics, with a dominance of subsidence regimes (see fig. 11a). Most models actually overestimate the maximum of occurence of weakly subsiding regimes. The others (CNRM-CM5 and INMCM4) overestimate the weakly ascending regimes, with hints of bimodality as documented in Oueslati and Bellon (2013b). In that study, a bimodal PDF of $\omega_{500}$ was attributed to feedbacks between large-scale circulation and deep convection that yield a strong double ITCZ bias. The models overestimate precipitation in all vertical regimes, particularly so in the ascending regimes (see fig. 11b). The largest contribution to observed precipitation in the tropics derives from weak-to-moderate ascent and weak subsidence, with a maximum for $\omega_{500}$ in the -30 to -10 hPa day$^{-1}$range (see fig. 11c). The majority of CMIP5 AGCMs capture the observed dominance of precipitation in weak-to-moderate ascent and weak subsidence. However, most of them overestimate the contribution of these particular regimes to precipitation (e.g., INMCM4, CNRM-CM5, IPSL-CM5A-LR...). In order to quantify the model error in representing the relationship between tropical circulations and precipitation, the normalized CPCE (Combined Precipitation Circulation Error) index is proposed as follows:

$$CPCE = \frac{\sqrt{\sum_{-80 \leq \omega \leq 80} (\Delta(PDF_{\omega} \times P_{\omega}))^2}}{\sum_{-80 \leq \omega \leq 80} (PDF_{obs} \times P_{obs})} \tag{2}$$

where $\omega$ is the monthly-mean mid-tropospheric (500hPa) vertical pressure velocity $\omega_{500}$, $PDF_{\omega}$ is the PDF of $\omega_{500}$, $P_{\omega}$ is the average precipitation for each $\omega_{500}$ regime, $P_{obs}$ and $PDF_{obs}$ are the observed distributions and $\Delta$ is the difference between the model and the observed distributions.

The purpose of the CPCE index is to quantify the errors in representing the interaction between precipitation and large-scale circulation in the tropics in order to understand their influence on precipitation biases in the DI region. To do so, the CPCE index should account for the large-scale properties of the DI region. In fact, one important difference between the distribution of vertical speed over the tropical belt and that in the DI region is the rare occurrence of strong ascending regimes ($\omega_{500} <$-60 hPa day$^{-1}$) in the latter. Strongly ascending motions occur mostly within large regions of deep convection such as the warm pool and monsoon region. Based on this observation, the CPCE is computed for vertical regimes whose frequency of occurence is higher than 0.01 in the DI region, accounting, therefore, for regimes that are important in the DI region and significant for the double ITCZ error. These regimes correspond to $\omega_{500}$ between -80 and 80 hPa day$^{-1}$. Indeed, we tried to release this hypothesis and found that the results presented hereafter were not as strong, due to the additional error and inter-model spread from the strongly ascending regimes that are not relevant to the DI syndrom. Because they are infrequently observed, parameterized convection in these regimes is poorly constrained, resulting in large biases and inter-model spread.

The relationship between the CPCE index and the double ITCZ error in AGCMs is shown in figure 12. It appears that INMCM4 presents the largest CPCE index and is considerably distant from the rest of the models. A careful analysis of residuals, leverage and Cook's distance of the regression presented in the Appendix objectively shows that INMCM4 is an outlier. Geoffroy et al. (2012) also diagnosed the anomalous character of INMCM4 when analyzing the global thermal properties of CMIP5 models. It thus seems reasonable to exclude INMCM4 in the following analyses.

A strong linear relationship between the CPCE and SI indexes can be seen in figure 12 and the correlation between the two is 0.85 (slightly larger than the correlation between the SI and THR-MLT). The linear regression between the SI and the CPCE in AGCMs can be written as:

$$SI = \alpha_0 + \alpha_2\ CPCE + \epsilon, \tag{3}$$

where $\alpha_0 = SI_{obs} + \epsilon_0$, with $\epsilon_0 = -0.25$ mm day$^{-1}$ and $\alpha_2 = 14.6$ mm day$^{-1}$ . $\alpha_2$ is statistically significant (the p value of the corresponding statistical test is smaller than $10^{-3}$). The regression results are summarized in Table 3.

The linear regressions described by Equations (1) and (3) show that in AGCMs, both THR-MLT and the CPCE can explain the spread in SI. Since AGCMs have the same SST forcing, both indexes are measures of the interaction between dynamics and precipitation. They are highly correlated at the -0.7 level and therefore carry overlaping information. However, comparing $\overline{R^2}$ between the two regression models, we can see that $\overline{R^2}$ in the regression model defined by Equation (3) is higher than that defined by Equation (1) ($\overline{R^2} = 0.7$ instead of 0.5). Also, the unexplained bias in the regression defined by Equation (3) is smaller than the unexplained bias in the regression defined by Equation (1) ($\epsilon_0 = -0.25$ mm day$^{-1}$ instead of 0.86 mm day$^{-1}$ ). Therefore, the SI spread between CMIP5 AGCMs appears better accounted for by the statistical model defined by Equation (3).

To further clarify the relative roles contributed by large-scale dynamics (CPCE) and local SST (THR-MLT) on the double ITCZ bias (SI) in AGCMs and OAGCMs, the next section is dedicated to a regression analysis on both predictors.

## 6 Respective roles of SST and circulation-precipitation interaction in the double ITCZ bias

The interaction between SST, large-scale dynamics and precipitation is examined by performing a multiple linear regression of the SI on both THR-MLT and CPCE in a manner similar to Bellon et al. (2010):

$$SI = \alpha_0 + \alpha_1\ (THR - MLT) + \alpha_2\ CPCE + \epsilon, \tag{4}$$

where $\alpha_0 = SI_{OBS} - \alpha_1(THR - MLT)_{OBS} + \epsilon_0$ is the intercept, $\alpha_1$ and $\alpha_2$ are regression coefficients and $\epsilon$ is the residual.

The statistical significance of the coefficients $\alpha_1$ and $\alpha_2$ is checked by Student's statistical test of the null hypothesis $H_0$ against an alternative hypothesis $H_1$ defined as:

$H_0:\ \alpha_i = 0$ ($\alpha_j$ being estimated);

$H_1: \ \alpha_i \neq 0$ ($\alpha_j$ being estimated);

with (i,j)=(1,2) or (2,1).

The results of the regression are summarized in Table 4.

## 6.1 AGCMs

The regression of the SI index is performed for AGCMs. Only $\alpha_2$ is statistically significant at the 98% confidence level (the p value associated to the statistical test is 0.02) and it is estimated at 10.6 mm day$^{-1}$ . The p value on the regression coefficient for THR-MLT is superior to 0.05. The null hypothesis for $\alpha_1$ is therefore accepted and the regression model proposed by Equation (4) reduces to the one of Equation (3). This shows that the error on the SST threshold THR between ascending and subsiding regimes appears to provide information on the SI error that is included in the error CPCE on the distribution of the vertical regimes' contribution to precipitation.

## 6.2 OAGCMs

### *6.2.1 The CPCE index in OAGCMs*

Dynamics-precipitation interaction is the driver of the double ITCZ bias in AGCMs. Given the unability of THR-MLT to explain entirely the double ITCZ bias in OAGCMs, it seems interesting to investigate the role of the large-scale atmosheric processes and see whether the CPCE provides additional information on the SI index in OAGCMs.

The $\omega_{500}$ regime sorting approach is applied for CMIP5 models. The obtained distributions are shown in figure 13. OAGCMs produce the same characteristics as the corresponding AGCMs in $\omega_{500}$ regime frequency and precipitation magnitude for individual regimes (see figs. 11 and 13), with the exception of IAP-FGOALS-g2 that slightly underestimates precipitation in strong ascent and overestimates precipitation in weak subsidence. Indeed, alike AMIP simulations, CMIP ones overestimate the contribution of weak-to-moderate ascent and weak subsidence to the total tropical precipitation (e.g., INMCM4, GISS-E2-R, CNRM-CM5...). These similar charateristics between the two model configurations reveal that errors on the precipitation large-scale dynamics relationship is an intrinsic error of AGCMs essentially independent of coupled feedbacks.

Based on the shape of the weighted precipitation distribution, The CMIP5 models can be gathered into three groups (Bellucci et al, 2010). The first collects the majority of models which capture the observed dominance of precipitation in weak-to-moderate ascent and weak subsidence. The second group collects models displaying two relative maximas, in both ascending and subsiding regimes (IPSL-CM5A-LR, IPSL-CM5A-MR, MIROC5 and CSIRO-Mk3-6-0). The third group corresponds to models which exhibit a maximum contribution to precipitation in subsiding regimes. This group only includes IAP-FGOALS-g2. Despite the erroneous maximum, IAP-FGOALS-g2 produces a realistic representation of precipitation in regimes of moderate and strong ascending motions.

The role of dynamics-precipitation interaction on the double ITCZ in OAGCMs is examined by displaying the CPCE index as a function of the SI index (see fig. 14). Again INMCM4 is identified as an outlier (see fig. 18a in the Appendix) and excluded from the following analyses. Unlike in the AMIP simulations, no obvious link appears between the CPCE and the SI in OAGCMs. The correlation between the CPCE and the SI is 0.3. By itself, the CPCE is unable to explain the inter-model spread of the double ITCZ bias in the CMIP simulations. But it is interesting to investigate whether the CPCE provides additional information to THR-MLT. The multiple linear regression of the SI on both THR-MLT and CPCE (described by Eq. (4)) is thus performed.

In both cases, $H_0$ can be rejected at the 95% confidence level. This shows that, in OAGCMs, THR-MLT and the CPCE provide independent and complementary information on the SI index. The coefficient $\alpha_1$ is estimated to -0.77 mm day$^{-1}$ $^{\circ}C^{-1}$ (with a p value of about $10^{-6}$), a value similar to the regression on THR-MLT only (see Eq. (1)) ; this shows that the CPCE and THR-MLT provide information that overlap very little (indeed, the correlation between THR-MLT and the CPCE is 0.03). The linear regression provides the following estimates: $\alpha_2 = 7.3$ mm day$^{-1}$ (with a p value of $5.10^{-3}$), $\alpha_0 = 2.8$ mm day$^{-1}$ and $\epsilon_0 = 0.7$ mm day$^{-1}$ .

The robustness of this regression model as well as the appropriateness of excluding INMCM4 is verified by checking each model residuals, leverage and Cook's distance (see fig. 18 in the Appendix).

The regression model in Equation (4) provides a more complete set of drivers of the double ITCZ than the model of Equation (1). This is illustrated by the increased adjusted $R^2$ ($\overline{R^2}$). $\overline{R^2} = 0.85$ in the regression model defined by Equation (4) instead of 0.7 in that defined by Equation (1). In addition, the unexplained bias is smaller than in Equation (1) ($\epsilon_0 = 0.7$ mm day$^{-1}$ instead of 1.3 mm day$^{-1}$ ), showing that a larger part of the error on the SI is better accounted for by the statistical model defined by Equation (4). However, $\epsilon_0 \neq 0$ show that some mechanisms are still missing to explain completely the double ITCZ bias and further investigation is needed.

To summarize the different contributions to the SI bias in OAGCMs, we rewrite Equation (4) to express the SI bias:

$$\Delta SI = \alpha_1 \; \Delta(THR - MLT) + \alpha_2 \; CPCE + \epsilon + \epsilon_0, \tag{5}$$

where $\Delta$ indicates the difference between the model and the observed values. This decomposition of the SI bias in OAGCMs are shown in figure 15.

Models producing pronounced double ITCZ bias (e.g. GISS-E2-R, MRI-CGCM3, GFDL-ESM2M...) show significant and positive errors in representing both atmospheric and coupled processes. Combined, these errors result in a larger SI bias. In contrast, models producing a smaller SI bias (e.g. MIROC5, IPSL-CM5A-LR, IPSL-CM5A-MR) show a negative bias on THR-MLT, that compensates the error on the simulated relationship between circulation and convection. In these models, SST and associated coupled feedbacks described by THR-MLT play a compensatory role on atmospheric processes. This, explains, in particular, the larger SI produced in the AMIP simulations of MIROC5 compared to the CMIP simulations. This is not the case in IPSL-CM5A-LR and IPSL-CM5A-MR, where the SI bias is amplified in CMIP simulations, which suggests that other coupled processes are misrepresented in OAGCMs that are not accounted for by the THR-MLT index. Overall, it appears that the misrepresentation of the interaction between convection and circulation (as measured by the CPCE) explains a significant fraction of the SI bias, but the error on coupled processes (as measured by THR-MLT) explains most of the inter-model spread.

Tables 2, 3 and 4 summarize the results of the performed regressions.

**Table 2** Results of the regression of the SI on THR-MLT (Equation (1))

| **Eq 1** | $\alpha_1$ | **p value** | $\epsilon_0$ | $\overline{R^2}$ |
|---|---|---|---|---|
| AMIP | -0.82 | $1\ 10^{-3}$ | 0.86 | 0.5 |
| CMIP | -0.83 | $1\ 10^{-5}$ | 1.3 | 0.7 |

**Table 3** Results of the regression of the SI on the CPCE (Equation (3))

| **Eq 3** | $\alpha_2$ | **p value** | $\epsilon_0$ | $\overline{R^2}$ |
|---|---|---|---|---|
| AMIP | 14.6 | $5\ 10^{-4}$ | -0.25 | 0.7 |

**Table 4** Results of the regression of the SI on THR-MLT and the CPCE (Equation (4))

| **Eq 4** | $\alpha_1$ | **p value** | $\alpha_2$ | **p value** | $\epsilon_0$ | $\overline{R}^2$ |
|---|---|---|---|---|---|---|
| AMIP | -0.34 | 0.16 | 10.6 | 0.02 | 0.03 | 0.71 |
| CMIP | -0.77 | $7\ 10^{-7}$ | 7.3 | $5\ 10^{-3}$ | 0.7 | 0.85 |

*6.2.2 Decomposition of the weighted precipitation bias in OAGCMs*

A more detailed description of the precipitation-large-scale circulation interaction can be obtained by decomposing the weighted precipitation bias in each CMIP5 model into three terms:

$$\Delta(PDF_\omega \times P_\omega) = \Delta PDF_\omega \times P_{obs} + \Delta P_\omega \times PDF_{obs} + \Delta PDF\omega \times \Delta P\omega \tag{6}$$

where $PDF_\omega$ is the $\omega_{500}$ PDF, $P_\omega$ is the average precipitation for each $\omega_{500}$ regime, $P_{obs}$ and $PDF_{obs}$ are the observed distributions and $\Delta$ indicates the difference between the model and the observed values. The first term corresponds to the error in the PDF. It is associated with the circulation bias. The second term corresponds to the bias resulting from the errors of precipitation simulated in each dynamical regime, considered to be the thermodynamical contribution. The third term is associated with the covariation of dynamical and thermodynamical biases. The contributions to the weighted precipitation bias, ordered with ascending CPCE index, are shown in figure 16. The model IPSL-CM5B-LR, whose CPCE index is the lowest (see fig. 14), produces the most realistic representation of the precipitation-large-scale circulation relationship through a compensation between dynamical and thermodynamical errors in ascending and subsiding regimes.

A common characteristic between the other CMIP5 models appears within weak-to-moderate ascending regimes (-60 $< \omega_{500} <$0 hPa day$^{-1}$): comparing the shape of the different distributions, it appears that the error on the weighted precipitation ($\Delta(PDF_\omega \times P_\omega)$) is controlled by the error in the frequency of occurence of vertical regimes ($\Delta PDF_\omega \times P_{obs}$), rather than the error in precipitation intensity within each regime ($\Delta P_\omega \times PDF_{obs}$). Models with small CPCE (e.g., BCC-CSM1-1, CSIRO-Mk3-6-0...) tend to underestimate the frequency of weak-to-moderate ascending regimes and overestimate precipitation intensity in these regimes, resulting in a compensation between the two errors and a more realistic contribution of weak-to-moderate ascending regimes to the mean tropical precipitation. However, models with larger CPCE index (e.g., CNRM-CM5, GISS-E2-R,...) overestimate both the precipitation and the frequency of occurence of weak-to-moderate ascending regimes. This combination of errors is pointed out in Oueslati and Bellon (2013b) as strongly associated with the double ITCZ bias.

Under strong ascending regimes ($\omega_{500}$ <-60 hPa day$^{-1}$), the error in regime frequency is less important and it is the error in precipitation intensity that determines the amplitude of the weighted precipitation error. These regimes, however, play a minor role on the double ITCZ problem as already mentioned.

Two model behaviors can be distinguished regarding the contribution of subsiding regimes to the total precipitation. Most models show realistic distributions, resulting from a compensation between dynamical and thermodynamical errors (e.g., MOHC-HadGEM2-ES). The others present larger errors, which, with the exception of IAP-FGOALS-g2, are explained by dynamical errors (e.g., MIROC5).

To summarize, errors in the precipitation-dynamics relationship are mostly due to errors in the frequency of occurence of vertical regimes, rather than errors in precipitation intensity within each regime (Bellucci et al, 2010; Oueslati and Bellon, 2013b). Errors in regime frequency are associated with an overestimated frequency of both weak-to-moderate ascending regimes and subsiding regimes. However, only the error in weak-to-moderate ascending regimes is most likely to influence the double ITCZ error. The overestimated frequency of subsiding regimes, instead, tends to suppress deep convection through lower tropospheric drying.

## 7 Summary and conclusions

This study examines the double ITCZ problem in CMIP5 (Coupled Model Intercomparaison Project phase 5) OAGCMs and AGCMs. The monthly outputs of 21 years (1979-1999) of simulations from 17 OAGCMs are analyzed, together with the 13 available AMIP simulations.

The results show that all the models still suffer from the double ITCZ bias to some extent, with a too-zonally elongated SPCZ and a spurious ITCZ in the Eastern Pacific. Since CMIP3, the simulation of the ITCZ has improved only in a few models, either through increased resolution (IPSL-CM5A, CNRM-CM5, MPI-ESM-LR) or improved convection parametrization (NCAR-CCSM4, IPSL-CM5B-LR). The seasonal cycle of the precipitation in the Eastern Pacific has improved in some models compared to Dai (2006) and De Szoeke and Xie (2008). But, over the central Pacific, most models still produce a persistent double ITCZ error, with a southern rainbelt present throughout the year. Indeed, comparing the Southern ITCZ (SI) index, it appears that the double ITCZ bias has become small in AMIP simulations, and that coupled atmosphere-ocean feedbacks still account for a large part of this bias in CMIP simulations, similarly to the previous generations of models (Lin, 2007).

The present study proposes a method to quantify the respective roles of SST and large-scale dynamics in the double ITCZ problem based on a linear regression analysis.

The role of SST and the associated coupled feedbacks is examined through the THR-MLT index (Bellucci et al, 2010). This index estimates the likelihood for a given model to yield deep convection in the DI region, combining biases on the representation of local most frequent SSTs (MLT) and the SST threshold leading to the onset of ascent (THR) in the DI region. The high correlation between THR-MLT and the SI found in CMIP3 models (Bellucci et al, 2010) is verified in the new generation of OAGCMs (with a correlation coefficient of -0.89), showing that the double ITCZ problem is mainly thermodynamically driven by the local SSTs in southeastern Pacific. However, performing a simple regression between the SI and THR-MLT, it appears that THR-MLT does not explain entirely the double ITCZ bias. Also, the interaction between THR-MLT and the SI is not as strong in AGCMs with a correlation at the -0.7 level. In addition, since AMIP simulations have the same oceanic forcing, THR-MLT is directly controlled by THR, in contrast with OAGCMs where it is strongly determined by the model SST biases. Among the mechanisms controlling THR, feedbacks between precipitation and large-scale dynamics play a dominant role.

The error on the simulated relationship between large-scale vertical motion can be measured by the Combined Precipitation Circulation Error (CPCE). This index is defined using the mid-tropospheric vertical velocity $\omega_{500}$ sorting methodology (Bony et al, 2004) in the tropics (30°S-30°N) and combines biases on the frequency of occurence of vertical regimes and on the rainfall magnitude associated with each individual regime. In AGCMs, the relationship between the SI and the CPCE is stronger than that between the SI and the THR-MLT, with a correlation coefficient of 0.87. This shows that the SI spread between AGCMs is better accounted for by the CPCE and points out the important role played by precipitation-large-scale dynamics interaction in the double ITCZ bias. In fact, large-scale circulation can promote or suppress convection through ascending and subsiding motions, modifying the vertical heating profile and the moisture-convection feedbacks (e. g. Lau et al (1997); Hirota et al (2011); Oueslati and Bellon (2013b)). Deep convection, in turn, can force the large-scale circulation by modifying the pressure gradients through moist diabatic processes (Gill, 1980; Oueslati and Bellon, 2013a). The role of the error on the simulated interaction between precipitation and dynamics in coupled ocean-atmosphere simulations is investigated by performing a multiple linear regression of the SI on both THR-MLT and CPCE. This new regression model provides a significantly more complete description of the SI than a regression on THR-MLT alone.

The precipitation bias in southeastern tropical Pacific is driven by biases on local thermodynamical coupled processes associated with SST and on the global characteristics of the dynamical mechanisms associated with the precipitation-circulation interaction. The coupled processes account in particular for the inter-model spread. In some models (MIROC5, IPSL-CM5A-LR, IPSL-CM5A-MR), coupled processes biases described by THR-MLT reduce the double ITCZ bias. It results, in the case of MIROC5, in a smaller SI bias in CMIP simulations compared to AMIP simulations.

The errors in the precipitation-dynamics relationship are dominantly caused by overestimated frequency of occurence of weak-to-moderate ascending regimes, rather than by errors in precipitation intensity within each regime (Bellucci et al, 2010; Oueslati and Bellon, 2013b). This suggests that processes inhibiting deep convection (e. g. convective entrainment, downdrafts and large-scale subsidence) are still poorly represented in CMIP5 models. A better representation of some observed negative feedbacks on convection can help alleviate the double ITCZ. In particular, in some models (e. g. IPSL-CM5A-LR, IPSL-CM5A-MR, NCC-NorESM1-M), the smaller double ITCZ bias is explained by an overestimated frequency of subsiding regimes, that tends to suppress deep convection through lower-tropospheric drying.

Our analysis suggests that the THR-MLT (Bellucci et al, 2010) and the CPCE indexes are relevant metrics to quantify the biases on SST and large-scale dynamics in OAGCMs and AGCMs that affect the double ITCZ bias. But they fail to explain completely the bias on SI. More efforts toward the construction and the use of such metrics are needed to evaluate climate model performance.

**Acknowledgements** We would like to thank Aurélien Ribes for helpful discussions. We also acknowledge the World Climate Research Programme's Working Group on Coupled Modelling, which is responsible for CMIP, and we thank the climate modeling groups (listed in Table 1 of this paper) for producing and making available their model output. For CMIP the U.S. Department of Energy's Program for Climate Model Diagnosis and Intercomparison provides coordinating support and led development of software infrastructure in partnership with the Global Organization for Earth System Science Portals.

## Appendix

### Evaluating the Results of a Linear Regression

To validate the results of a linear regression, it is important to examine the residuals ($\epsilon$) from the regression and identify extreme data points (leverage), that can potentially exercise a great influence on the regression line. The residuals are normalized (i.e., divided by the standard deviation of the residuals) in order to make the analysis on a standard scale.

The leverage is based on how the observed values differ from the values predicted by the regression model: $\hat{SI} = H\ SI$, where $SI$ is the vector of observed values, $\hat{SI}$ is the vector of values predicted by the regression model and $H$ is the hat matrix. The leverage of the i-th value is the i-th diagonal element ($h_{ii}$) of the hat matrix $H$.

Combining both residuals and leverage, we obtain a measure of the actual influence each point has on the slope of the regression line, namely the Cook's distance. Cook's distance is a measure of the effect of deleting a given observation on the regression analysis (Cook and Weisberg, 1982).

Cook's distance is calculated as: $D_i = \frac{\sum_{j=1}^{n}(\hat{SI}_j - \hat{SI}_{j(i)})^2}{p\ MSE}$, where $\hat{SI}_j$ is the prediction from the full regression model for observation $j$, $\hat{SI}_{j(i)}$ is the prediction for observation $j$ from a refitted regression model in which observation $i$ has been omitted, $MSE$ is the mean square error of the regression model and $p$ is the number of parameters in the model. Cook's distance can be expressed as a function of both residuals and leverage: $D_i = \frac{\epsilon_i^2}{p\ MSE}[\frac{h_{ii}}{(1-h_{ii})^2}]$, where $\epsilon_i$ is the residual of the regression. Data points with large residuals and/or high leverage may alter the result of the regression.

Smaller Cook's distances means that removing the observation has little effect on the regression results. Distances larger than 1 are suspicious and suggest the presence of a possible outlier or a poor model.

Figure 17 shows the standardised residuals versus leverage plot of the regression model, described by Equation (3), performed with AGCMs, with and without INMCM4. The relationship between residuals and leverage is highlighted through a LOESS curve (LOcal regrESSion[2], Fox (2002)). Superimposed on the plot are contour lines for the Cooks distance.

Comparing the two plots, we see that the regression performed without INMCM4 (see fig. 17b) exhibit smaller residuals and leverage. Indeed, the values of Cook's distance are inferior to 1. This confirms the robustness of the regression model described by Equation (3) in AGCMs and validates the exclusion of INMCM4.

Figure 18 shows the same plot of the regression model, described by Equation (4), performed with

[2] LOESS denotes a method that is also known as locally weighted polynomial regression. At each point in the data set a low-degree polynomial is fitted to a subset of the data, with explanatory variable values near the point whose response is being estimated. The polynomial is fitted using weighted least squares, giving more weight to points near the point whose response is being estimated and less weight to points further away.

OAGCMs, with and without INMCM4. Again, INMCM4 is identified as an outlier (see fig. 18a). Indeed, after excluding INMCM4, residuals and leverage are smaller and the values of Cook's distance are inferior to 1 (see fig. 18b). This validates the regression model described by Equation (4) in OAGCMs and emphasizes its suitability at explaining the double ITCZ bias through both THR-MLT and CPCE indexes.

## References


Adler RF, Huffman GF, Chang A, Ferraro R, Xie P, Janowiak J, Rudolf B, Schneider U, Curtis S, Bolvin D, Gruber A, Susskind J, Arkin P, Nelkin E (2003) The version 2 global precipitation climatology project (GPCP) monthly precipitation analysis (1979-present). J Hydrometeorol 4:1147–1167

Arakawa A, Schubert WH (1974) Interaction of a cumulus cloud ensemble with the large-scale environment, Part I. Journal of the Atmospheric Sciences 31:674–701

Back L, Bretherthon C (2008) On the relationship between sst gradients, boundary layer winds and convergence over the tropical oceans. Journal of Climate 22:4182–4196

Bacmeister JT, Suarez MJ, Robertson FR (2006) Rain reevaporation, boundary layerconvection interactions, and pacific rainfall patterns in an AGCM. Journal of the Atmospheric Sciences 63:3383–3403

Bellon G, Gastineau G, Ribes A, Le Treut H (2010) Analysis of the tropical climate variability in a two-column framework. Climate Dynamics 37:73–81

Bellucci A, Gualdi S, Navarra A (2010) The double-ITCZ syndrome in coupled general circulation models: the role of large-scale vertical circulation regimes. Journal of Climate 5:1127–1145

Betts AK (1986) A new convective adjustment scheme. Part I: Observational and theoretical basis. Quarterly Journal of the Royal Meteorological Society 112:677–691

Bony S, Dufresne JL, Le Treut H, Morcrette JJ, Senior C (2004) On dynamic and thermodynamic components of cloud changes. Climate Dynamics 22:71–86

Bougeault P (1985) A simple parametrisation of the large scale effects of cumulus convection. Monthly Weather Review 4:469–485

Charney JG (1971) Tropical cyclogenesis and the formation of the ITCZ. In: Reid WH (ed) Mathematical problems of geophysical fluid dynamics, American Mathematical Society, pp 355–368

Chikira M (2010) A cumulus parameterization with state-dependent entrainment rate. part II: Impact on climatology in a general circulation model. Journal of the Atmospheric Sciences 67:2194–2211

Chikira M, Sugiyama M (2009) A cumulus parameterization with state-dependent entrainment rate. part I: Description and sensitivity to temperature and humidity profiles. Journal of the Atmospheric Sciences in press

Cook RD, Weisberg S (1982) Residuals and influence in regression. New York, NY: Chapman and Hall

Dai AG (2006) Precipitation characteristics in eighteen coupled climate models. Journal of climate 9:4605–4630

De Szoeke SP, Xie SP (2008) The tropical eastern pacific seasonal cycle: Assessment of errors and mechanisms in IPCC AR4 coupled ocean-atmosphere general circulation models. Journal of Climate 21:2573–2590

Del Genio AD, Yao MS (1993) Efficient cumulus parameterization for long-term climate studies: The giss scheme. American Meteorological Society pp 181–184

Derbyshire SH, Maidens AV, Milton SF, Stratton RA, Willett MR (2012) Adaptive detrainment in a convective parametrization. Quarterly Journal of the Royal Meteorological Society submitted

Emanuel KA (1991) A scheme for representing cumulus convection in large-scale models. Journal of the Atmospheric Sciences 48:2313–2329

Emanuel KA (1994) Atmospheric convection. Oxford University Press

Fox J (2002) Nonparametric regression: Appendix to an r and s-plus companion to applied regression

Geoffroy O, Saint-Martin D, Olivié DJL, Voldoire A, Bellon G, Tytéca S (2012) Transient climate response in a two-box 1 energy-balance model. part I: analytical solution and parameter calibration using CMIP5 AOGCM experiments. Journal of Climate submitted

Gill AE (1980) Some simple solutions for heat-induced tropical circulation. Quarterly Journal of the Royal Meteorological Society 106:447–462

Graham NE, Barnet TP (1987) Sea surface temperature, surface wind divergence, and convection over tropical ocean. Science 238:657–659

Grandpeix JY, Lafore JP (2010) A density current parameterization coupled with emanuel's convection scheme. Part I: The models. Journal of the Atmospheric Sciences 67(4):881–897

Grandpeix JY, Lafore JP, Cheruy F (2010) A density current parameterization coupled with emanuel's convection scheme. Part II: 1d simulations. Journal of the Atmospheric Sciences 67(4):898–922

Gregory D, Rowntree PR (1990) A mass flux convection scheme with representation of cloud ensemble characteristics and stability dependent closure. Monthly Weather Review 118:1483–1506

Gutzler DS, Wood TM (1990) Structure of large-scale convective anomalies over the tropical oceans. Journal of Climate 3:483–496

Hess PG, Battisti DS, Rasch PJ (1993) Maintenance of the inter-tropical convergence zones and the tropical circulation on a water-covered earth. Journal of the Atmospheric Sciences 50:691–713

Hirota N, Takayabu YN, Watanabe M, Kimoto M (2011) Preciptation reproducibility over tropical oceans and tis relationship to the double ITCZ problem in CMIP3 and MIROC5 climate models. Journal of Climate 24:4859–4873

Holton JR, Wallace JM, Young JA (1971) On boundary layer dynamics and the ITCZ. Journal of the Atmospheric Sciences 28:275–280

Hubert LF, Krueger AF, Winston JS (1969) The double intertropical convergence zone-fact or fiction? Journal of the Atmospheric Sciences 26:771–773

Lau KM, Wu HT, Bony S (1997) The role of large scale atmospheric circulation in the relationship between tropical convection and sea surface temperature. Journal of Climate 10:381–392

Lin JL (2007) The double-ITCZ problem in IPCC AR4 coupled GCMs: Ocean-atmosphere feedback analysis. Journal of Climate 18:4497–4525

Lindzen RS (1974) Wave-CISK in the tropics. Journal of the Atmospheric Sciences 31:156–179

Lindzen RS, Nigam S (1987) On the role of the sea surface temperature gradients in forcing the low-level winds and convergence in the tropics. Journal of the Atmospheric Sciences 44:2418–2436

Liu H, Lin P, Yu Y, Zhang X (2012) The baseline evaluation of LASG/IAP climate system ocean model (LICOM) version 2. Acta Meteor Sinica 26:318–329

Liu Y, Guo L, Wu G, Wang Z (2010) Sensitivity of the ITCZ configuration to cumulus convective parametrizations on an aquaplanet. Climate Dynamics 34:223–240

Mechoso CR, Robertson AW, Barth N, Davey MK, Delecluse P, Gent PR, Ineson S, Kirtman B, Latif M, Le Treut H, Nagai T, Neelin JD, Philander SGH, Polcher J, Schopf PS, Stockdale T, Suarez MJ, Terray L, Thual O, Tribbia JJ (1995) The seasonal cycle over the tropical pacific in coupled ocean-atmosphere general circulation models. Monthly Weather Review 123:2825–2838

Moorthi S, Suarez MJ (1992) The relaxed arakawa-schubert. a parametrization of moist convection for general circulation models. Mon Wea Rev 120:978–1002

Neale RB, Richter JH, Jochum M (2008) The impact of convection on ENSO: From a delayed oscillator to a series of events. Journal of Climate 21:5904–5924

Nordeng TE (1994) Extended versions of the convection parametrization scheme at ecmwf and their impact upon the mean climate and transient activity of the model in the tropics. ECMWF Tech Memo No 206

Numaguti A (1993) Dynamics and energy balance of the Hadley circulation and the tropical precipitation zones: Significance of the distribution of evaporation. Journal of the Atmospheric Sciences 50:1874–1887

Oueslati B, Bellon G (2013a) Tropical precipitation regimes and mechanisms of regime transitions: contrasting two aquaplanet general circulation models. Climate Dynamics 40:2345–2358

Oueslati B, Bellon G (2013b) Convective entrainment and large-scale organization of tropical precipitation: sensitivity of the CNRM-CM5 hierarchy of models. Journal of Climate 26:2931–2946

Pan DM, Randall DA (1998) A cumulus parametrization with a pronostic closure. Quarterly Journal of the Royal Meteorological Society 124:949–981

Rayner NA, Parker DE, Horton EB, Folland CK, Alexander LV, Rowell DP, Kent EC, Kaplan A (2003) Global analyses of sea surface temperature, sea ice, and night marine air temperature since the late nineteenth century. Journal of Geophysical Research - Atmospheres 108,4407

Richter JH, Rasch PJ (2008) Effects of convective momentum transport on the atmospheric circulation in the community atmosphere model, version 3. Journal of Climate 21:1487–1499

Song XL, Zhang GJ (2009) Convection parameterization, tropical pacific double ITCZ, and upper-ocean biases in the NCAR CCSM3. part I: Climatology and atmospheric feedback. Journal of Climate 22:4299–4315

Xie S, Hume T, Jakob C, Klein SA, MacCoy RB, Zhang M (2010) Observed large-scale structures and diabatic heating and drying profiles during twp-ice. Journal of Climate 23:57–79

Zhang C (2001) Double ITCZs. Journal of Geophysical Research - Atmospheres 106(11):11,785–11,792

Zhang GJ, McFarlane NA (1995) Sensitivity of climate simulations to the parameterization of cumulus convection in the Canadian Climate Center general circulation model. Atmos Ocean 33:407–446

Zhang GJ, Mu M (2005) Effects of modifications to the zhang-mcfarlane convection parameterization on the simulation of thetropical precipitation in the national center for atmospheric research community climate model, version 3. Journal of Geophysical Research - Atmospheres 110:D09,109

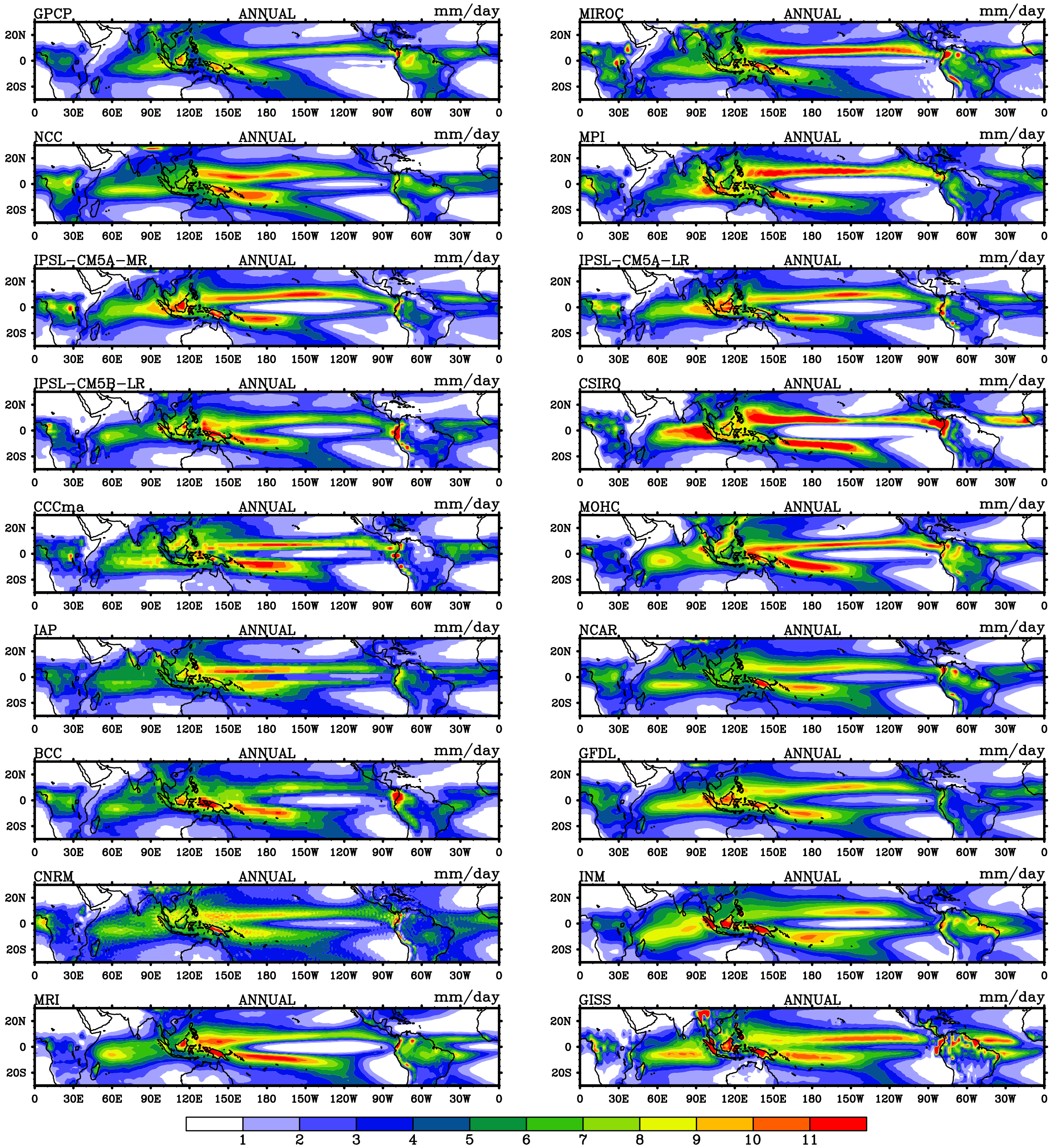


**Fig. 1** Annual mean precipitation (1979-1999) from GPCP data and 17 CMIP5 OAGCMs.

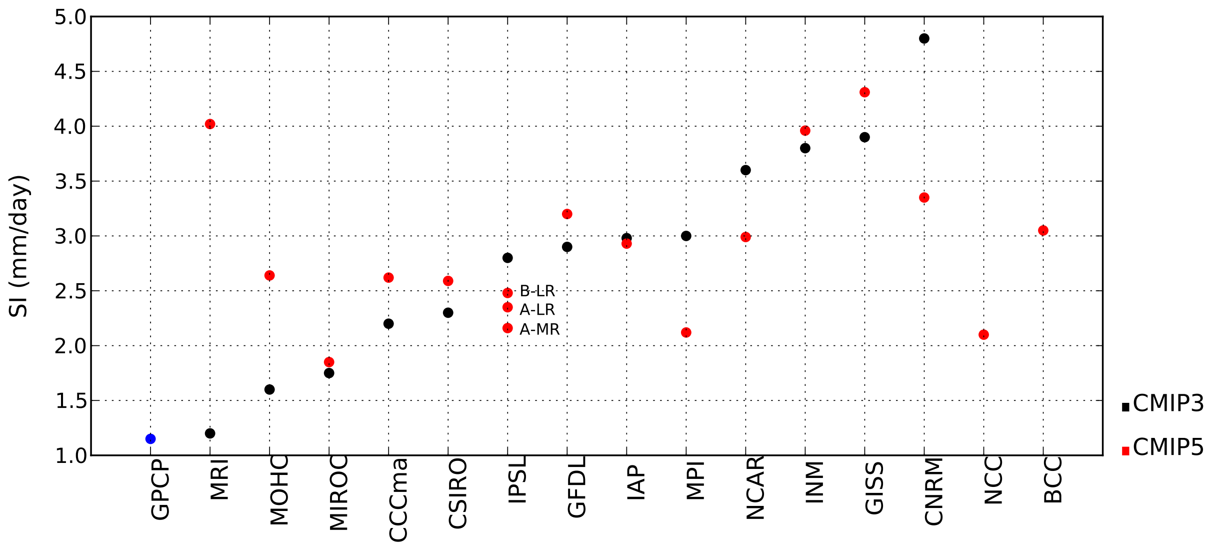


**Fig. 2** Southern ITCZ (SI) index for observations, CMIP3 and CMIP5 OAGCMs.

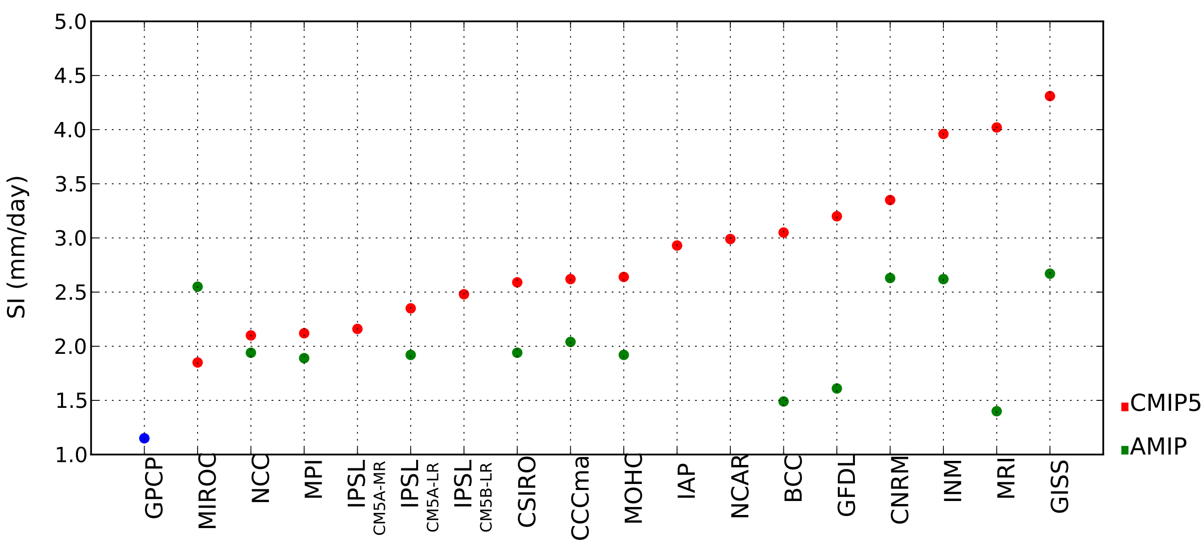


**Fig. 3** SI index for CMIP5 AGCMs (AMIP) and OAGCMs (CMIP).

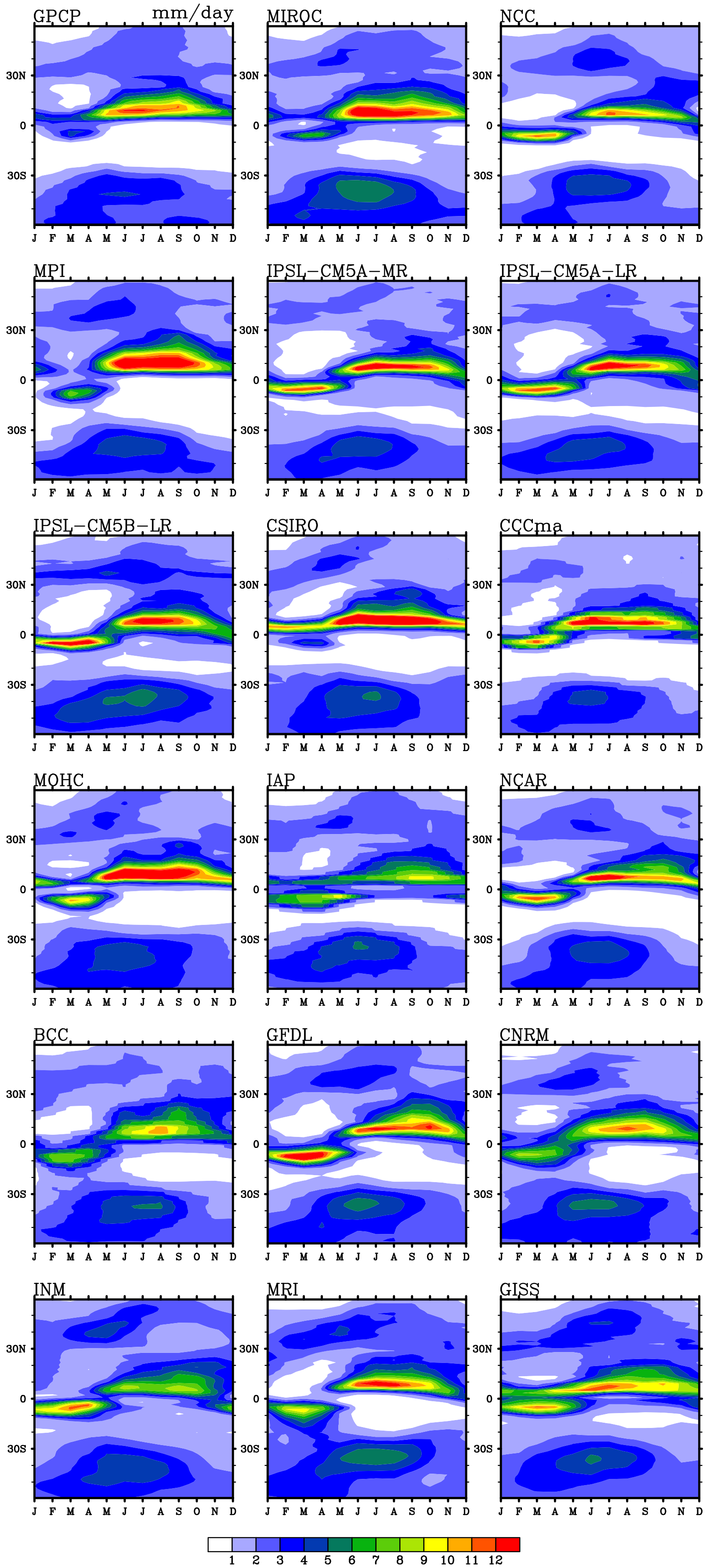


**Fig. 4** Seasonal cycle of precipitation in eastern Pacific (80W-120W) for GPCP data and CMIP5 OAGCMs.

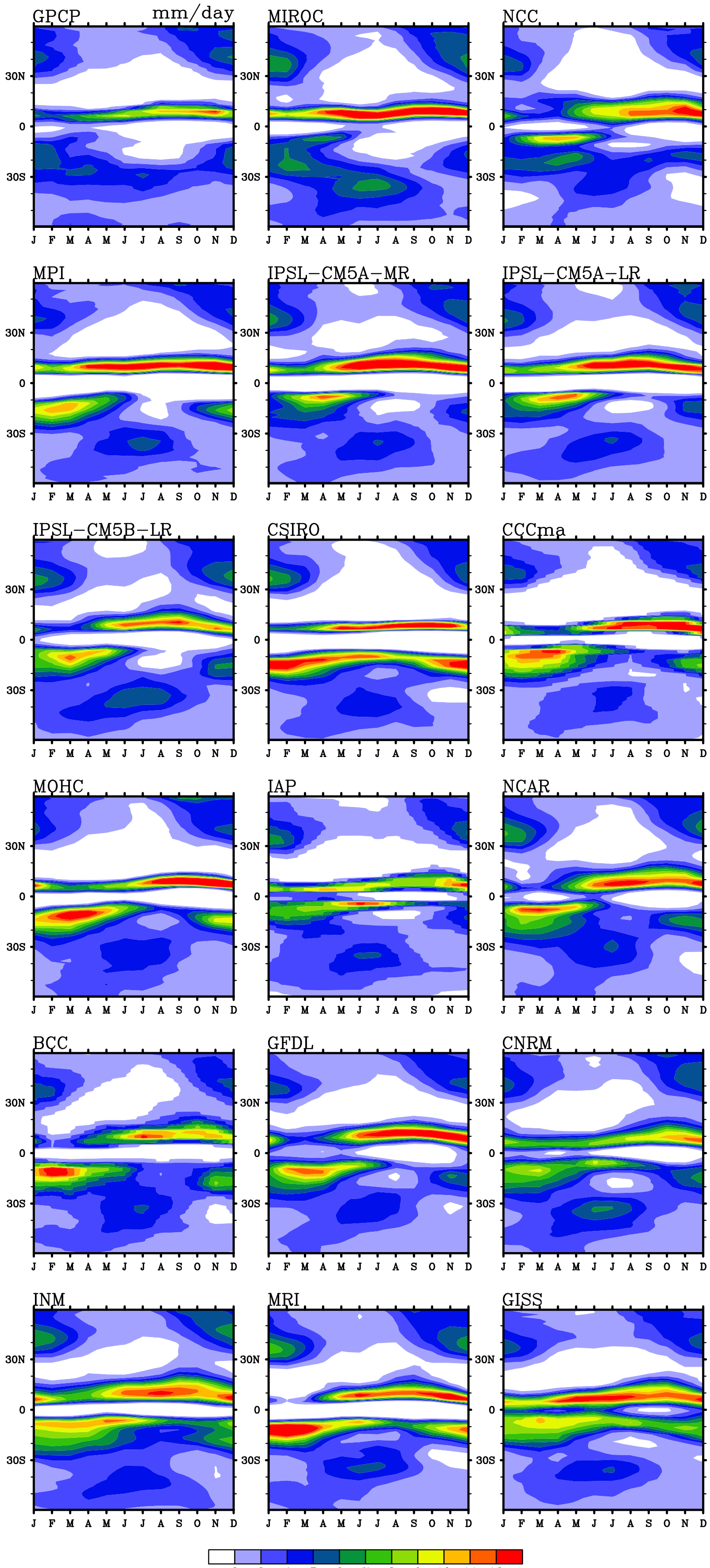


**Fig. 5** Seasonal cycle of precipitation in central Pacific (130W-170W) for GPCP data and CMIP5 OAGCMs.

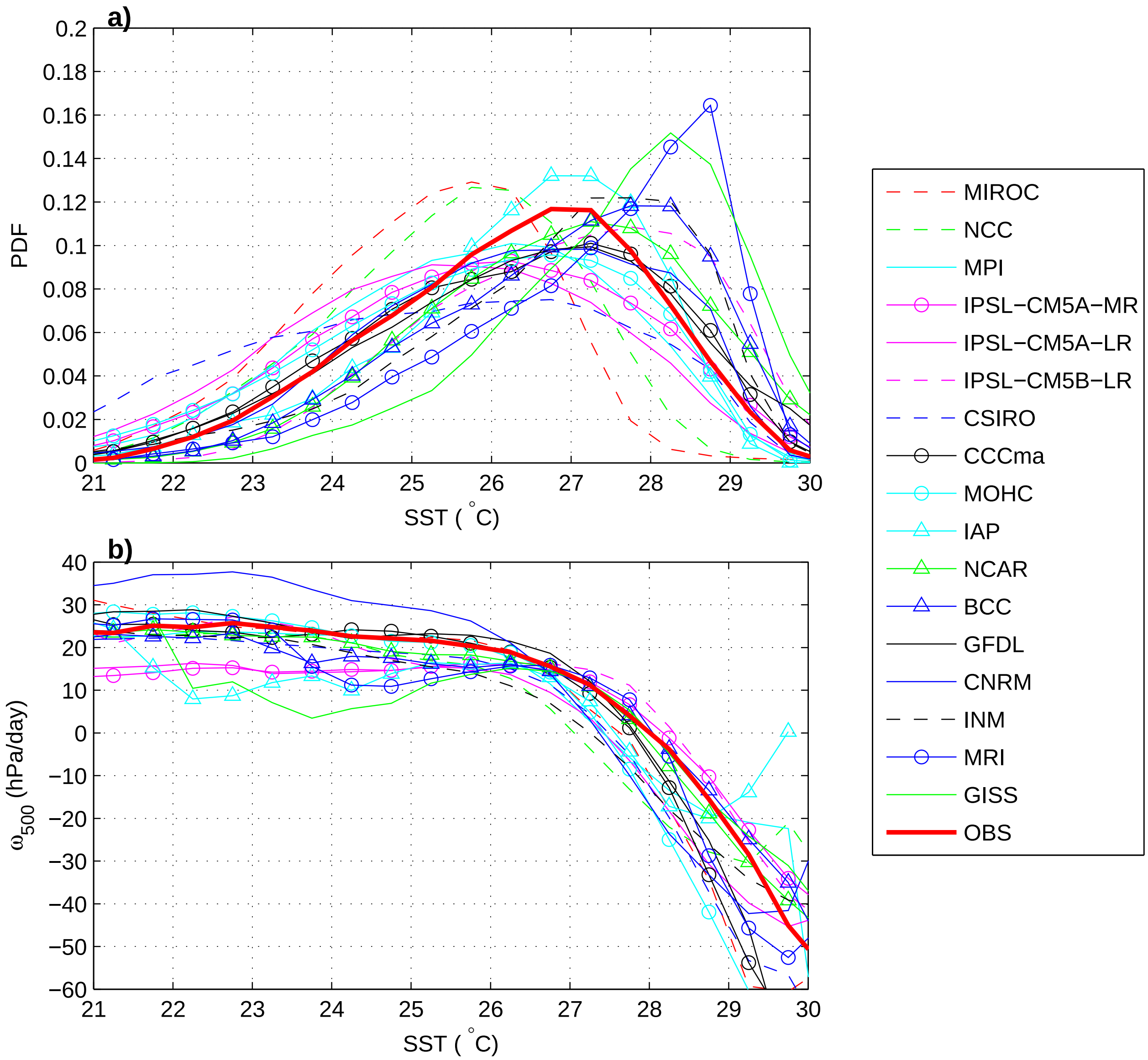


**Fig. 6** PDF of SST (a) and large-scale vertical velocity at 500 hPa $\omega_{500}$ as a function of SSTs (b) within 20°S-0°, 150°-100°W for CMIP5 OAGCMs.

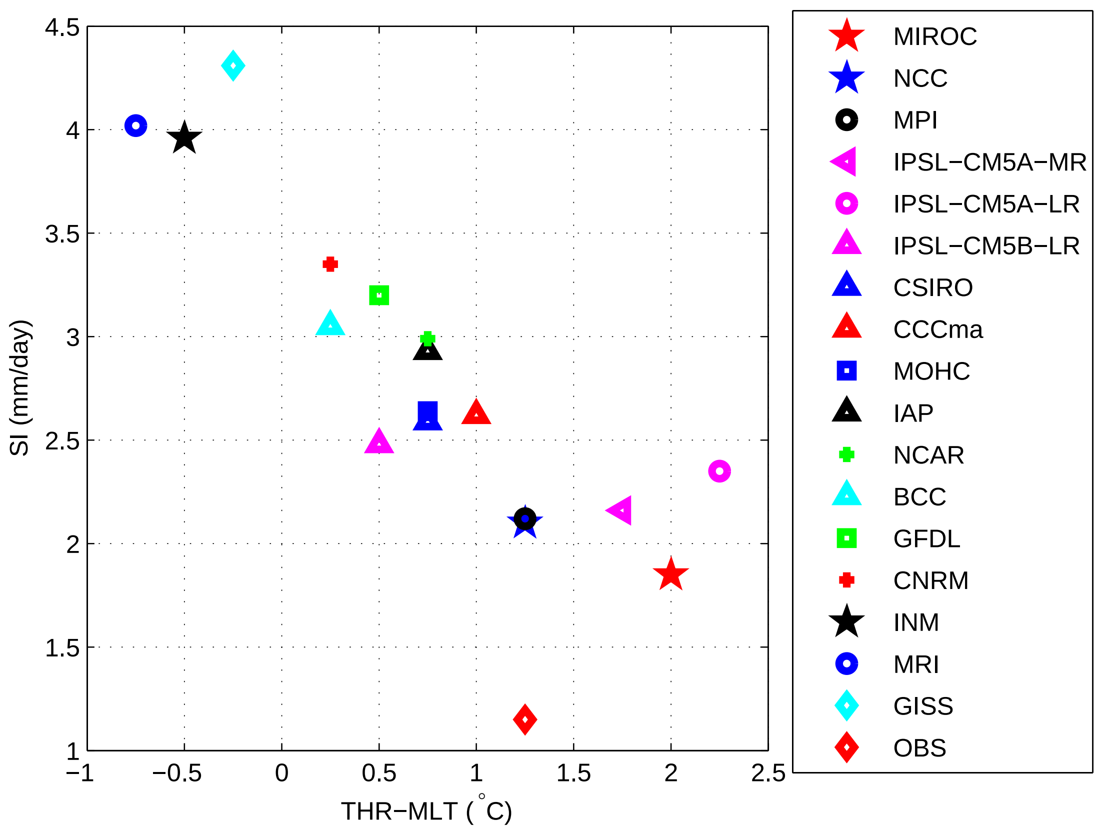


**Fig. 7** Scatterplot of THR-MLT and SI index for CMIP5 OAGCMs and observations.

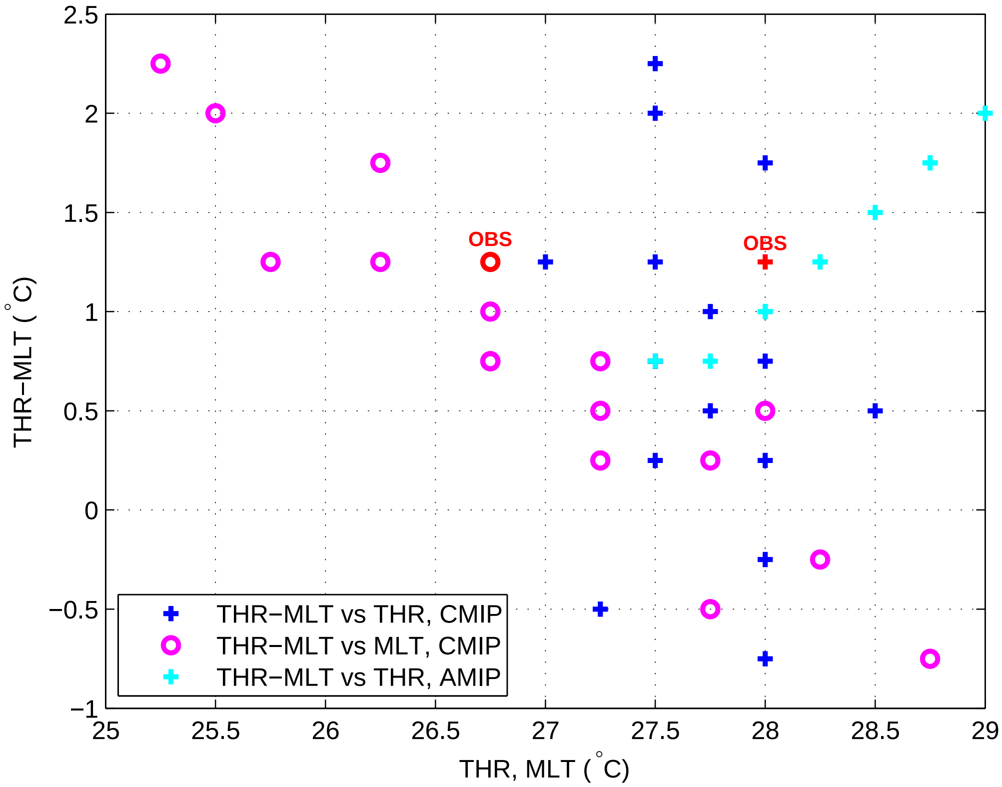


**Fig. 8** Scatterplot of THR-MLT and (THR, MLT) for observations, CMIP5 OAGCMs and AGCMs.

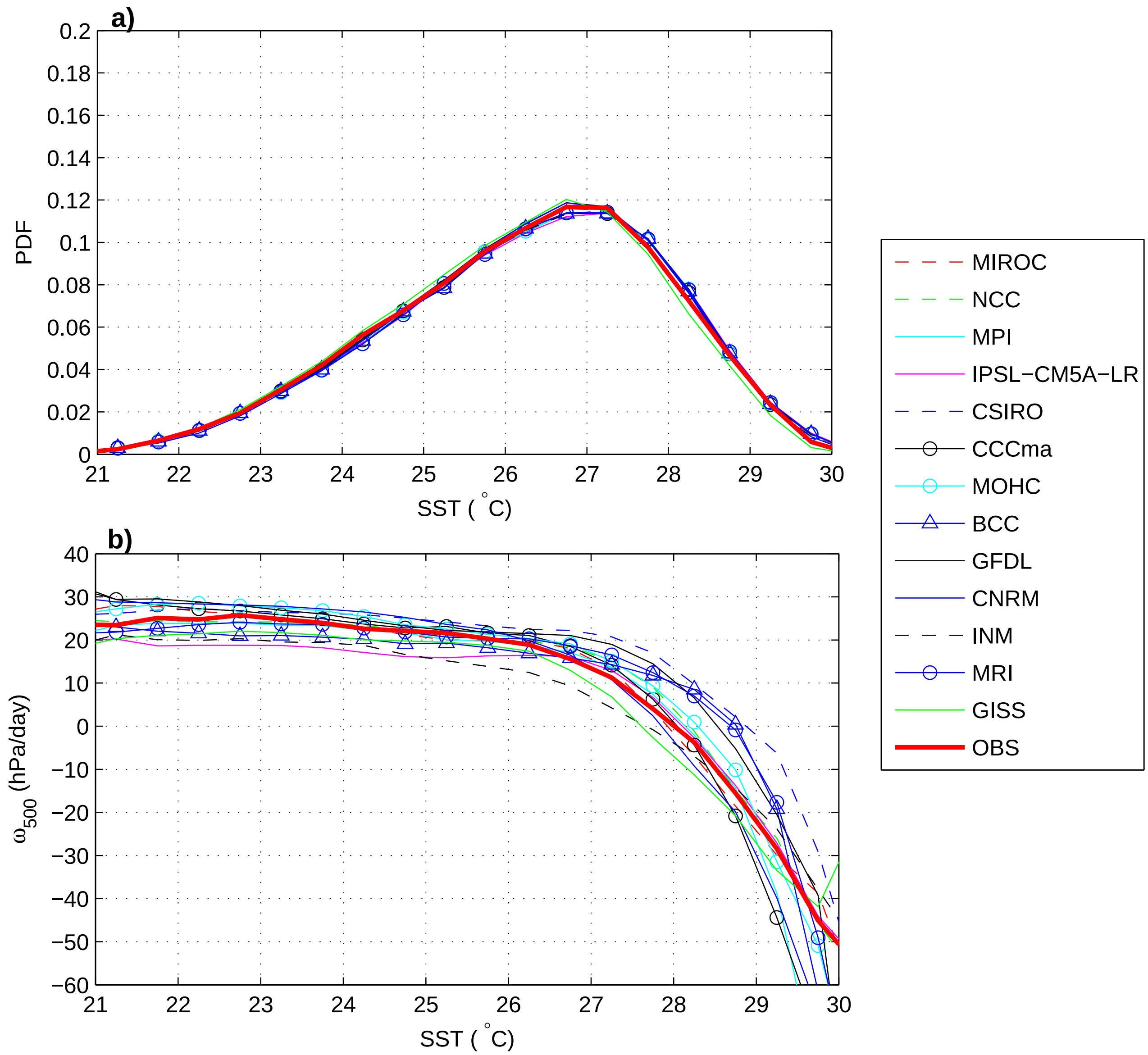


**Fig. 9** PDF of SST (a) and large-scale vertical velocity at 500 hPa $\omega_{500}$ as a function of SST (b) within 20°S-0°, 150°-100°W for observations and CMIP5 AGCMs

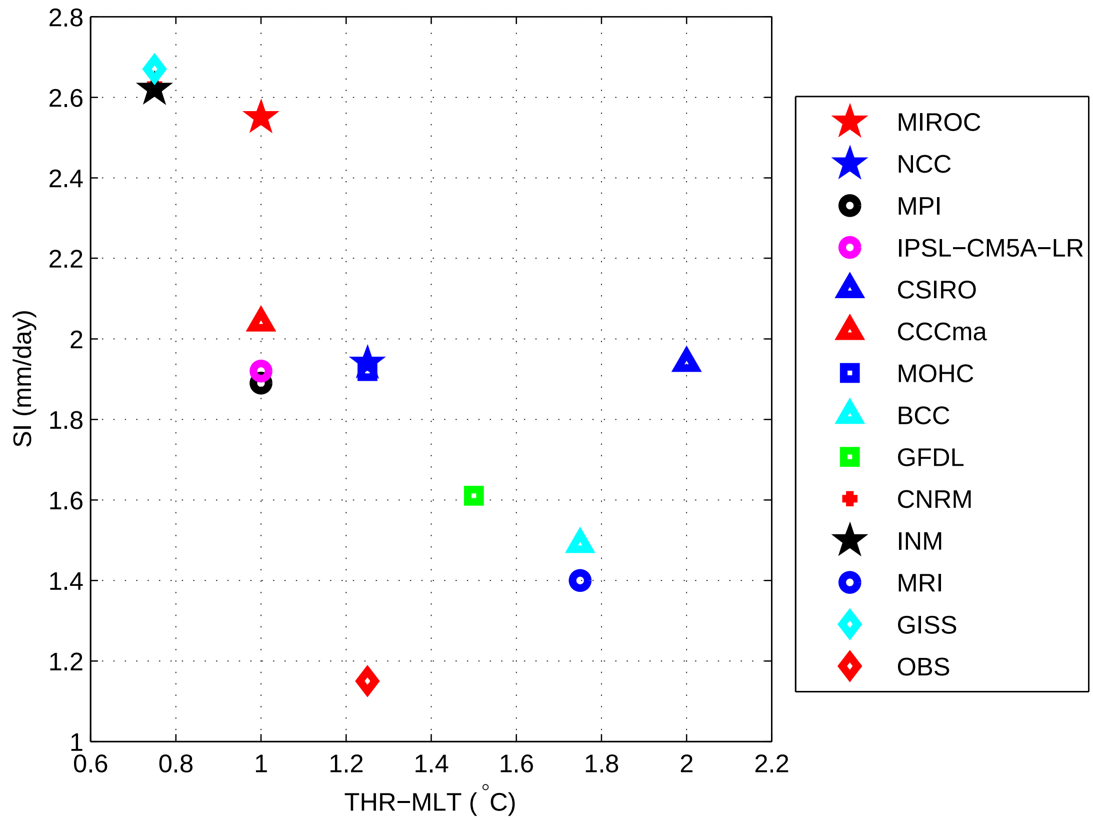


**Fig. 10** Scatterplot of THR-MLT and SI index for CMIP5 AGCMs and observations.

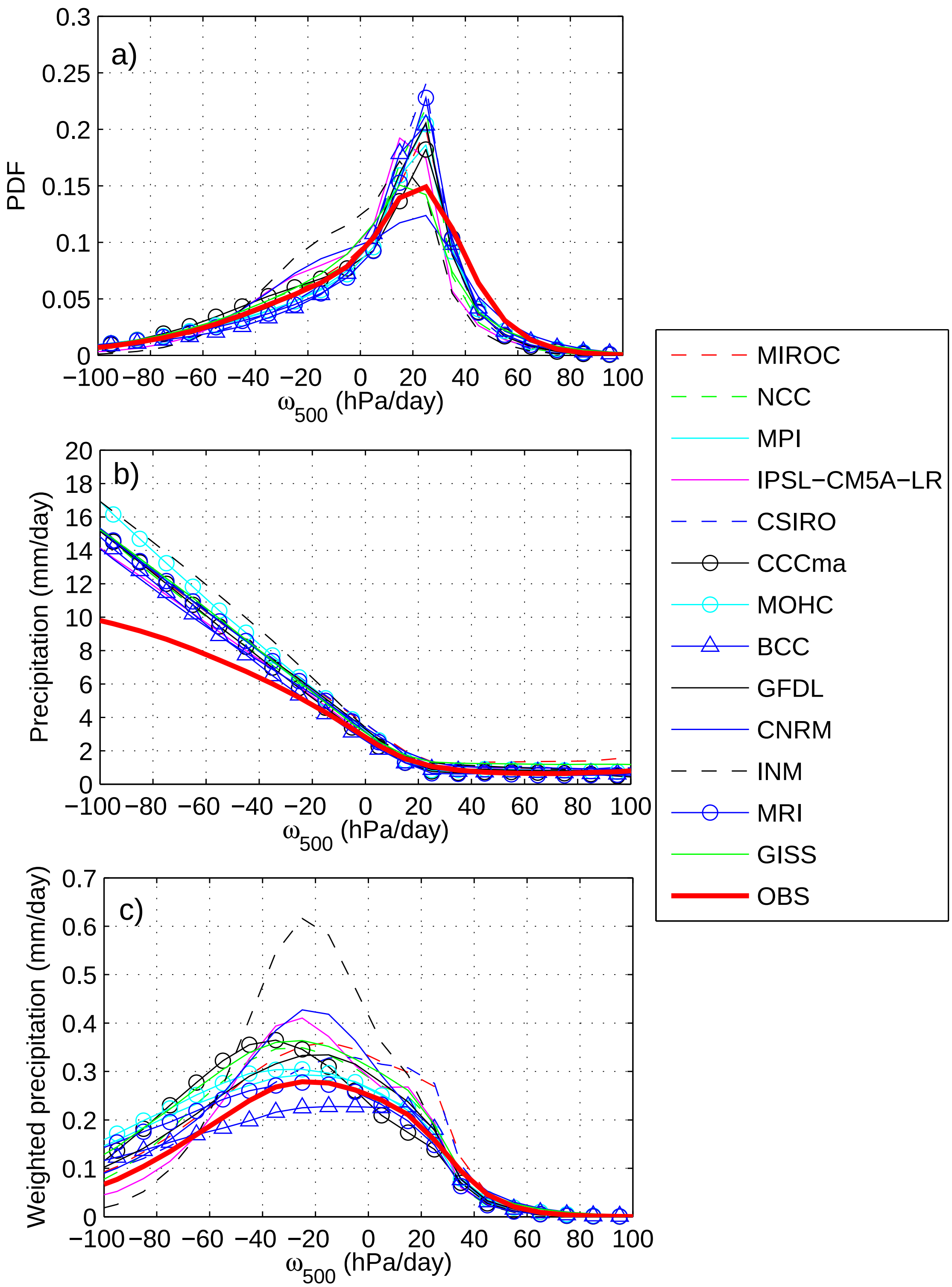


**Fig. 11** (a) PDF of the 500hPa large-scale vertical velocity $\omega_{500}$ in the tropics (30°S-30°N), (b) Precipitation as a function of $\omega_{500}$, (c) Contribution to the mean tropical precipitation as a function $\omega_{500}$, derived from observations and CMIP5 AGCMs.

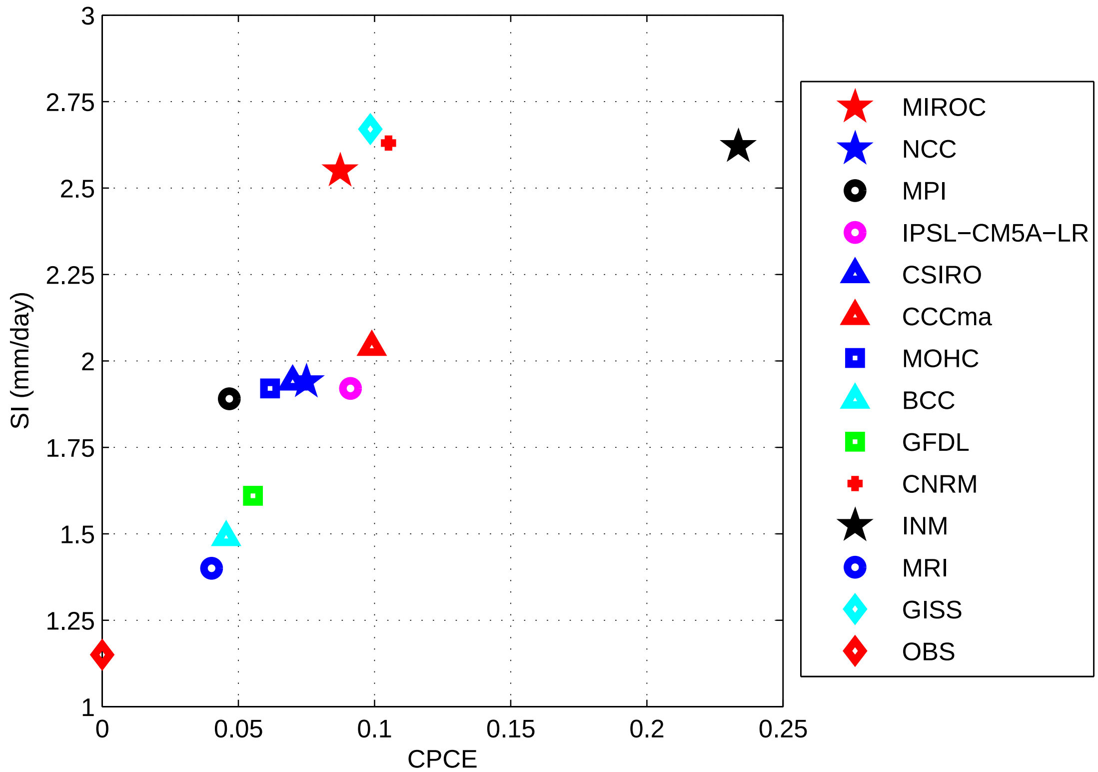


**Fig. 12** Scatterplot of CPCE and SI index for CMIP5 AGCMs and observations.

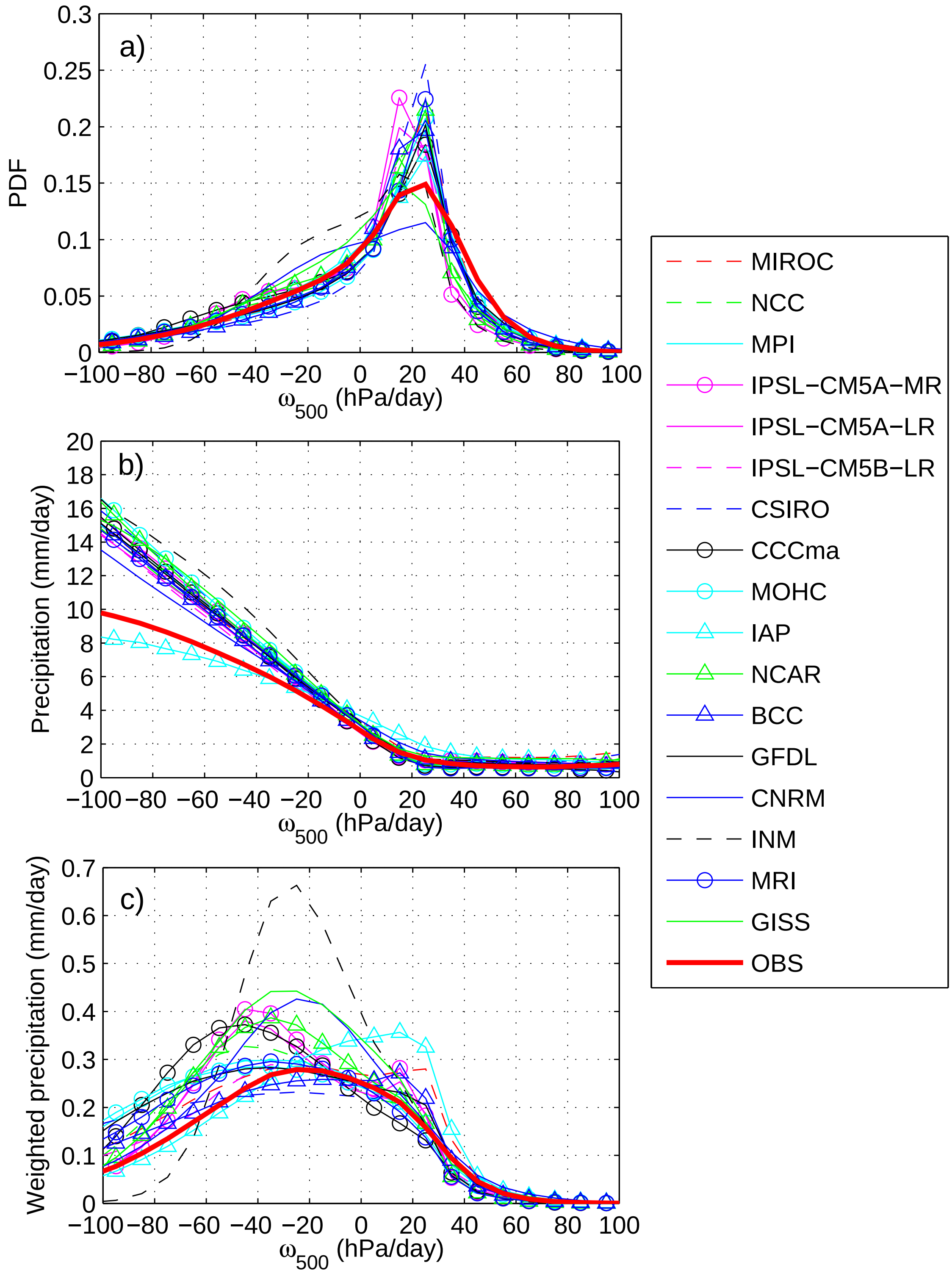


**Fig. 13** (a) PDF of the 500hPa large-scale vertical velocity $\omega_{500}$ in the tropics (30°S-30°N), (b) Precipitation as a function of $\omega_{500}$, (c) Contribution to the mean tropical precipitation as a function $\omega_{500}$, derived from observations and CMIP5 OAGCMs.

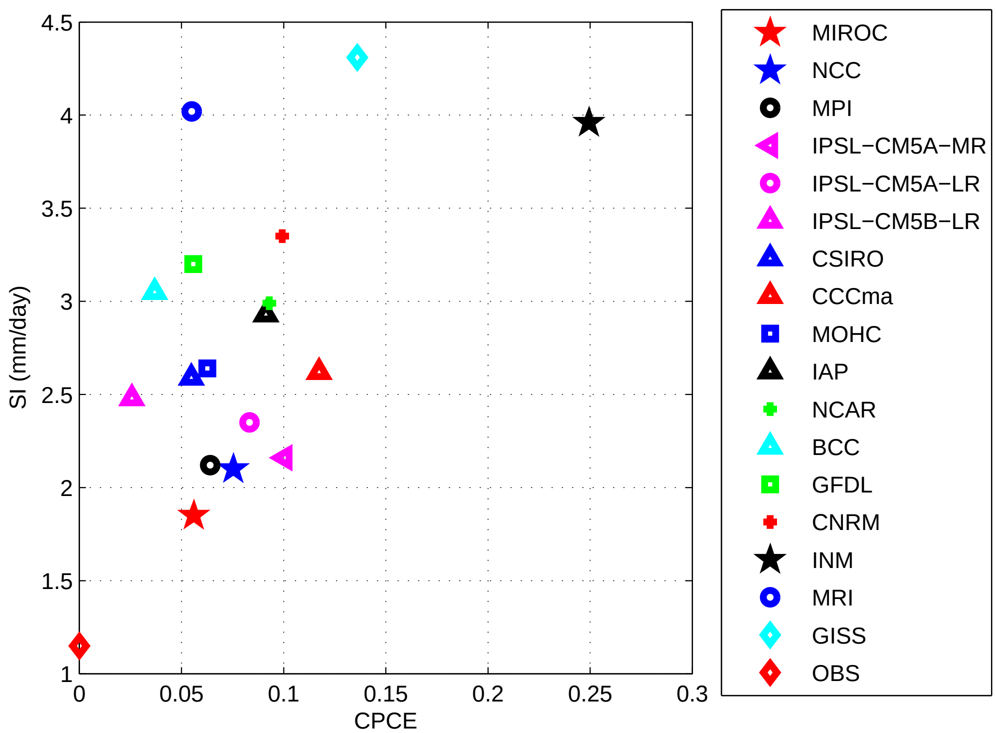


**Fig. 14** Scatterplot of CPCE and SI index for CMIP5 OAGCMs and observations.

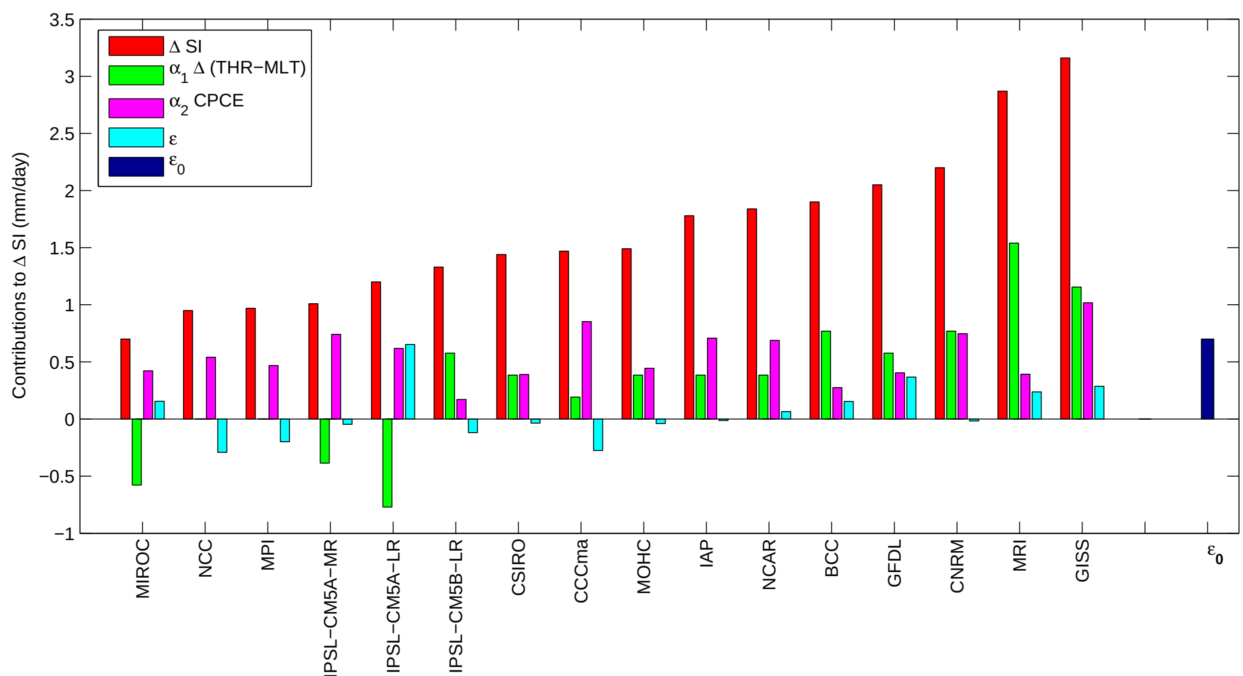


**Fig. 15** Contributions to the SI bias in OAGCMs computed from Equation (5).

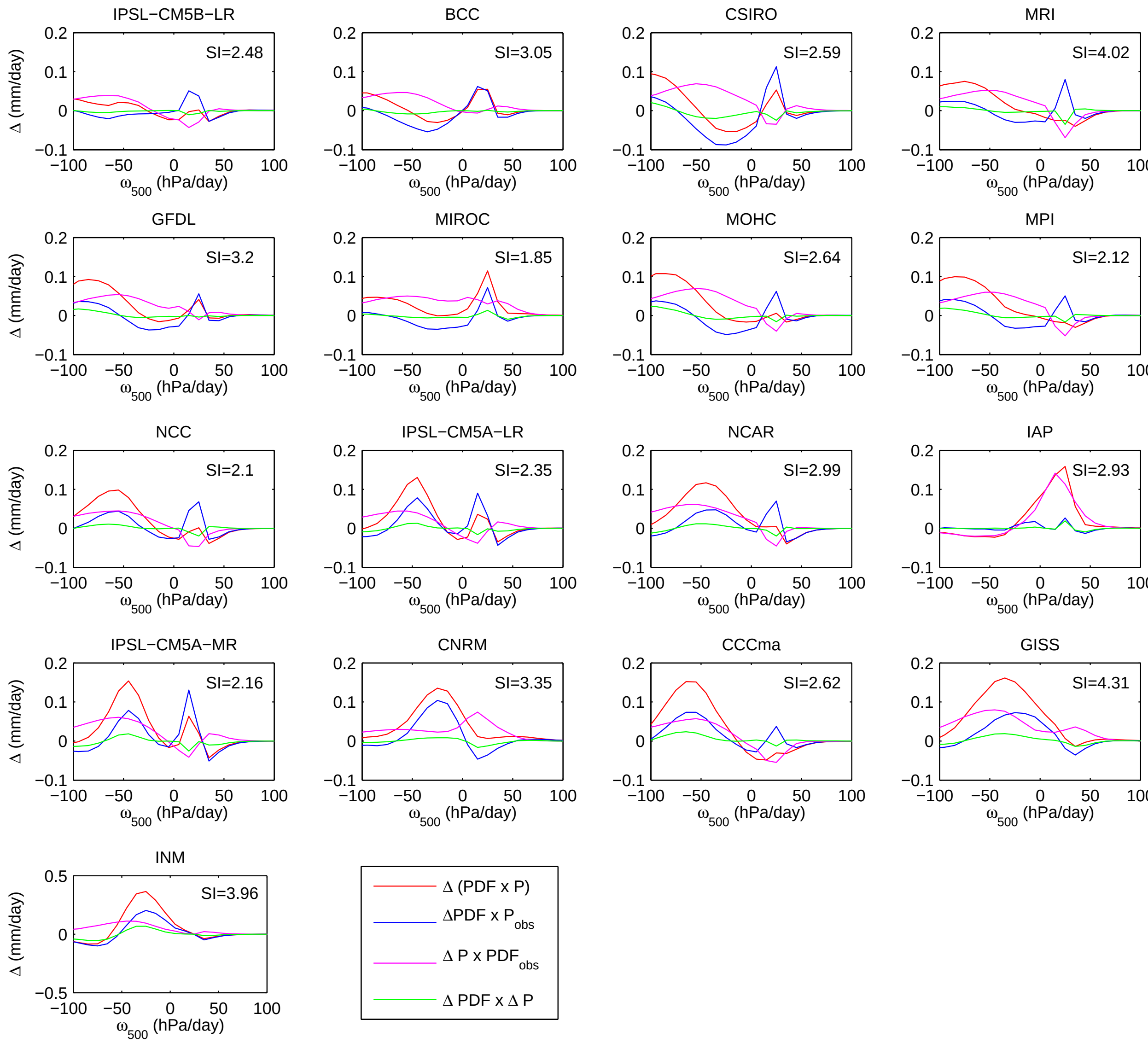


**Fig. 16** Decomposition of the weighted precipitation bias into three contributions from the PDF bias, the precipitation intensity bias and the co-variation of dynamic and non-dynamic biases.

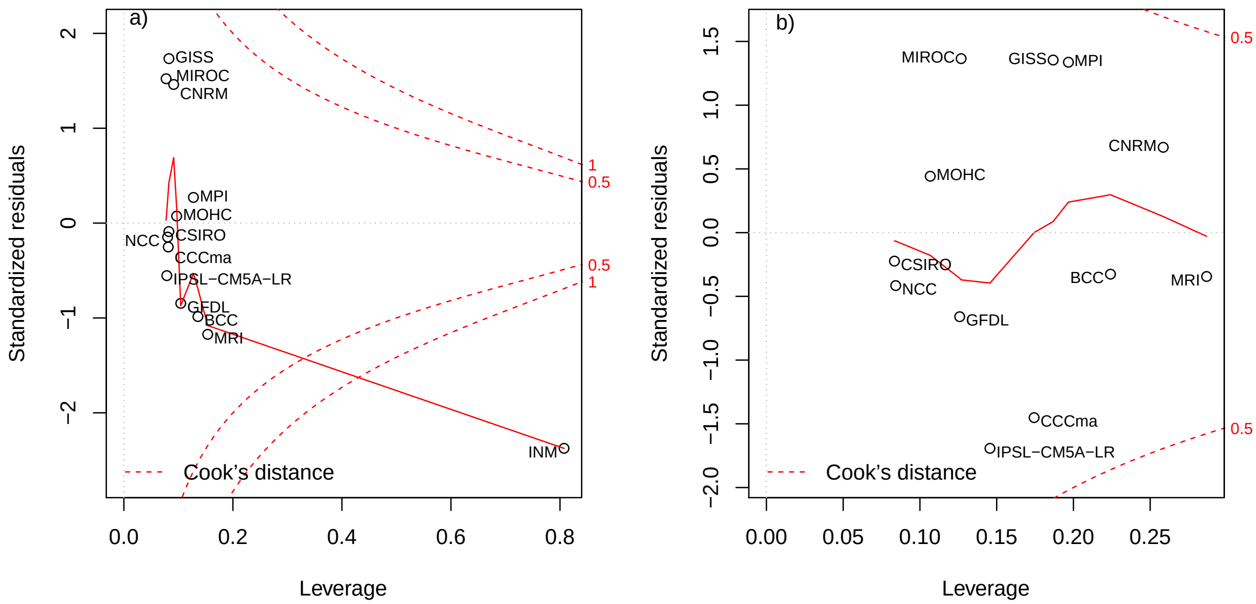


**Fig. 17** Standardised residuals versus leverage plot of the linear regression described in Equation (3), performed with atmoshpere-only models including (a) and excluding (b) INMCM4. The red line corresponds to the loess curve that fits to the scatter plot. Contour lines represent the Cook's distance.

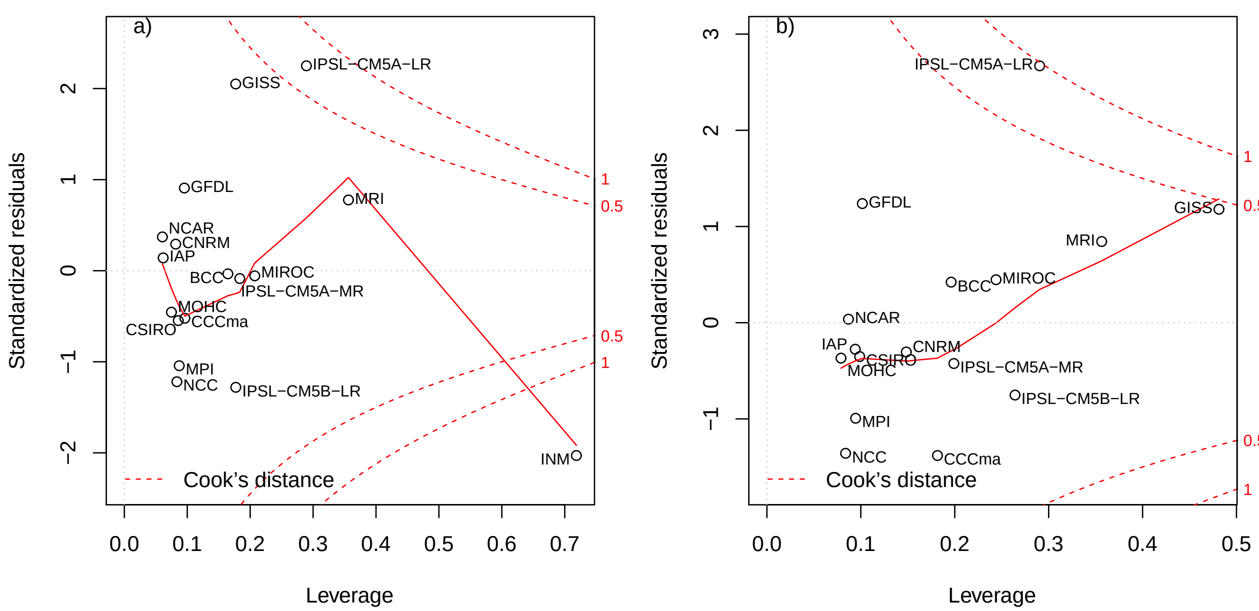


**Fig. 18** Standardised residuals versus leverage plot of the regression model described in Equation (4) including (a) and excluding (b) INMCM4. The red line corresponds to the loess curve that fits to the scatter plot. Contour lines represent the Cook's distance.